POLITECNICO DI MILANO
DEPARTMENT OF AEROSPACE ENGINEERING

POLITECNICO
MILANO 1863

Space Systems Engineering and Operations

AA 2023-2024

Professor: Michèle Roberta Lavagna

TEAM 13

Person Code	Surname	Name
10713569	Grandinetti	Roberta
10782473	Miccoli	Francesco Antonio
10765536	Mirri	Pietro
10776736	Natali	Martino
10730683	Nuccio	Gabriele
10768705	Righi	Laura

November 21, 2024

Contents

List of acronyms

SOHO	Solar and Heliospheric Observatory
LEO	Low Earth Orbit
MCC1	First Mid-course correction
MCC2	Second Mid-course correction
HOI	HALO Orbit Insertion
TTO	Transfer Trajectory Orbit
GOLF	Global Oscillations at Low Frequencies
VIRGO	Variability of Solar Irradiance and Gravity Oscillations
MDI	Michelson Doppler Imager
SOI	Solar Oscillations Investigation
CDS	Coronal Diagnostic Spectrometer
EIT	Extreme ultraviolet Imaging Telescope
LASCO	Large Angle and Spectrometric COronograph
SUMER	Solar Ultraviolet Measurements of Emitted Radiation
UVCS	UltraViolet Coronograph Spectrometer
SWAN	Solar Wind ANisotropies
CELIAS	Charge, Element, and Isotope Analysis System
COSTEP	COmprehensive Supra-Thermal and Energetic Particle analyzer
ERNE	Energetic and Relativistic Nuclei and Electron experiment
PS	Propulsion Subsystem
DTM	Dual Thruster Modules
CM	Center of Mass
CP	Center of Pressure
MR	Mass Ratio
TTMTC	Tracking, TeleMetry and TeleCommunication
ITU	InTernational communication Union
SNR	Signal to Noise Ratio
FOT	Flight Operations Team
MDI	Michelson Doppler Imager
BWA	Beam Waveguide Antenna
HEF	High Efficiency
R-S	Reed - Solomon
EIRP	Equivalent Isotropic Radiated Power
HPA	High Power Amplifier
HGA	High Gain Antenna
LGA	Low Gain Antenna

SS	Solid State
AOCS	Attitude, Orbit Control Subsystem
HR-STR	High Resolution Star Tracker
FPSS	Fine Pointing Sun Sensor
RW	Reaction Wheels
FSPAAD	Fine Sun Pointing Attitude Anomaly Detector
CSPAAD	Coarse Sun Pointing Attitude Anomaly Detector
ACU	Attitude Control Unit
ISA	Initial Sun Acquisition
ESR	Emergency Sun Reacquisition
FDE	Fault Detection Electronics
NM	Normal Mode
CRP	Coarse Roll Pointing
RMW	Rotating Momentum Wheels
SK	Station Keeping
MM	Momentum Management
SRP	Solar Radiation Pressure
PTCS	Payload module Thermal Control System
STCS	Service module Thermal Control System
TCS	Thermal Control Subsysystem
PLM	Payload Module
SVM	Service Module
MLI	Multi Layer Insulation
BSR	Back Surface Reflection
PCU	Power Control Unit
S3R	Sequential Switching Shunt regulator
BRU	Battery Regulator Unit
LCL	Latching Current Limit
TTP	Transfer Trajectory Phase
HOP	Halo Orbit Phase
SA	Solar Array
SO	Scientific Operations
DoD	Depth of Discharge
SAA	Solar Aspect Angle
PDU	Power Distribution Unit
DET	Direct Energy Transfer
PPT	Power Peak Tracking
FCL	Foldback current limit

PLM	Payload Module
MCC	Mid Course Correction
EPS	Electric Power Subsystem
ESR	Emergency Sun Re-acquistion
EOL	End Of Life
BOL	Begin Of Life
DSN	Deep Space Network
GSFC	Ground Service Facility Center
CDMU	Central Data Management Unit
CoM	Center of Mass
CPU	Central Process Unit
OBDH	On-Board Data Handling
PS	Propulsion Subsystem
RAM	Random Access Memory
ROM	Read Only Memory
RTU	Remote Terminal Unit
TMTC	Telemetry and Telecommunication
TP	Throughput
KIPS	Kilo-Instructions Per Second
MIPS	Mega-Instructions Per Second

1 SOHO mission

1.1 Introduction

SOHO is the longest-lived Sun-watching satellite to date. Since its launch on December 2^{nd} 1995, SOHO has revolutionized our understanding of the Sun. It has provided the first images of structures and flows below the Sun's surface and of activity on its far side. SOHO has revealed the Sun's extremely dynamic atmosphere, provided evidence for the transfer of magnetic energy from the surface to the outer solar atmosphere, the corona, and identified the source regions of the fast solar winds.
It has revolutionized our understanding of solar-terrestrial correlations and dramatically improved our space weather-forecasting by its uninterrupted stream of images covering the atmosphere, extended corona and far side.

1.2 High-level goals and Mission drivers

1.2.1 High-level goals

Understanding the changing Sun and its effects on the Solar System is one of the main goals of the SOHO mission, which was launched to address three fundamental science questions:

Scientific guiding questions	Mission goals
What is the structure and dynamics of the solar interior?	Probe the internal structure of the Sun through helioseismology
Why does the solar corona exist and how is it heated to the extremely high temperature of about 1 000 000 °C*?*	Characterise the strong and weak magnetic-field regions in the Sun's chromosphere and corona, analysis of the Sun spectrum focusing on UV region
Where is the solar wind produced and how is it accelerated?	Investigate the outflow of solar plasma and detailing the origin of the solar winds

Table 1: Mission objectives mapped from questions [44]

At the very beginning SOHO was designed for a nominal mission lifetime of two years. In 1997 the mission was extended until 2003 and then even forward because of its unprecedented success. The strategic plan proposed in 2003 came up with an additional goal answering to a new scientific question:

Scientific guiding question	Mission goal
What is the effect of the Sun on Earth weather?	Improve the prediction of climate and natural hazards, playing a lead role in the early warning system for space weather and evaluate the Sun impact over climate change.

Table 2: Additional mission goal [49]

1.2.2 Mission Drivers

Mission drivers are critical requirements that shape various aspects of the mission, including its goals, timeline, technology choices, budget, and overall strategy.
For the SOHO mission the following drivers were identified:

- **Communication with Earth shall be guaranteed**: for a mission to be considered a success, collected science data shall be transmitted back to Earth. For this purpose a pointable high gain antenna and a couple of deployed low gain ones ensure full coverage and communication with the Deep-Space Network ground stations. Moreover, effective communication plays a crucial role in aiding the ground segment operations for the satellite's Attitude Determination and Control System (ADCS). This necessity extends to fostering cooperation between the European Space Agency (ESA) and NASA in managing their respective ground segment operations. [50]
- **The Spacecraft shall achieve and maintain Sun pointing remaining in its operational HALO orbit**: mission goals focus entirely on the investigation of Sun's structure and dynamics,

from its inner core up to the external corona, and also involving solar wind phenomenon. Therefore, throughout the mission the spacecraft plays the role of an operational space solar observatory in halo orbit, which requires a three-axis attitude control during the Sun-pointing mode.
After full solar-panel deployment towards the Sun, elettric power supply will be ensured and the ADCS will perform the transition to fine Sun pointing and roll-angle control using a fine-pointing Sun sensor, a star tracker and three reaction wheels. It is in this configuration that the payload instruments will make their scientific observations, when the spacecraft's pointing towards the Sun is stabilised to within a few tenths of an arcsecond.
In order to maintain the halo orbit, which seems to best fit the mission objectives (as it will be outlined in Section 1.6), a series of stationkeeping maneuvers were optimally planned at eight week intervals using the 4 reaction wheels and the hydrazine thrusters during the RW momentum unloading.

1.3 Functional Analysis

1.3.1 Functional tree

A preliminary functional decomposition has to be carried out, aiming to properly identify the functionalities that need to be performed in order to meet the high level goals. The following Functional Tree provides a schematic representation of the mission, developed at different levels.

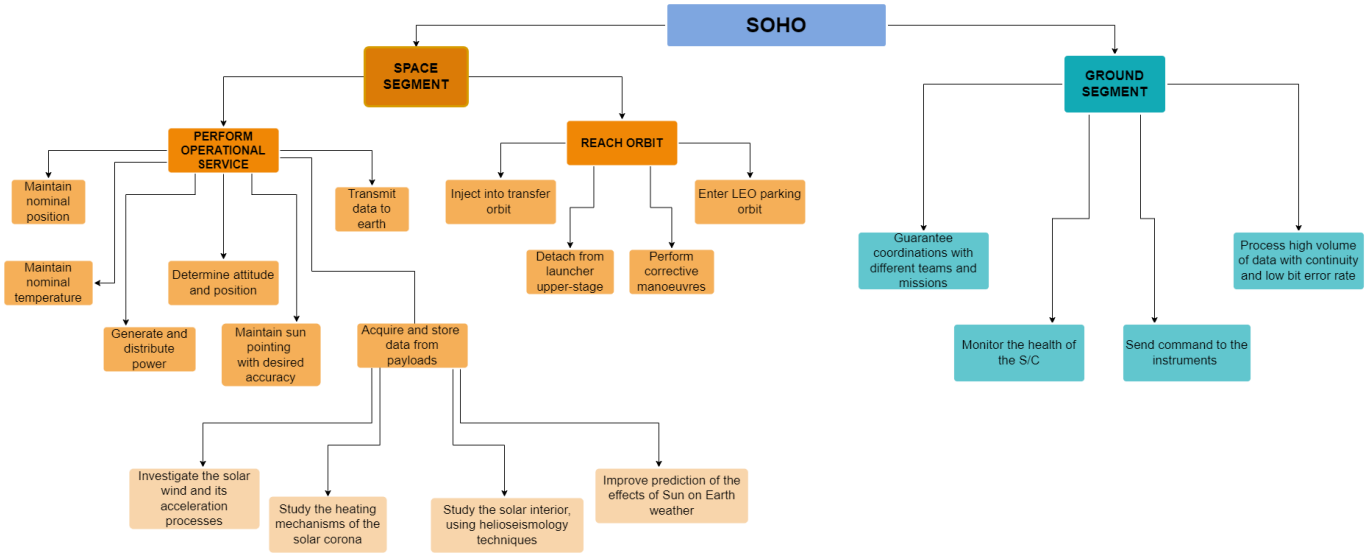

Fig. 1: Functional tree

1.3.2 Phases

The operational mission is divided into three main phases [47]:

1. **Launch and Early Orbit Phase (LEOP)**: This phase starts at lift-off, includes the coasting period in parking orbit, and ends with the injection of the spacecraft into the transfer trajectory. It is divided into two subphases:

   - Ascent Subphase: from lift-off until injection into parking orbit;
   - Parking-Orbit Subphase: from injection into parking orbit until injection into transfer trajectory.

   No communication with the ground is foreseen during this phase.

2. **Transfer Trajectory Phase (TTP)**: it starts with the injection of the spacecraft into transfer orbit and ends with the injection into the halo orbit. It lasts about 4 months and, although science operations should be possible and will likely occur, priority will given to the health and status of the spacecraft bus in this phase. It includes also an initial Sun acquisition, solar-array deployment up to 12 h after transfer trajectory insertion, and orbit-correction manoeuvres. The TTP is divided in the following four subphases:

- PRE-SEP: this lasts about 35 min from Transfer Trajectory Insertion (TTI) until separation from the Centaur upper stage, during which the first Acquisition of Signal (AOS) takes place;
- PRE-OP:this begins at separation and ends when the anti-Sun line/spacecraft/Earth angle is less than 33°. It should last about 3 h;
- LR: redundant low-gain antennas are both available for the low data rate;
- HR: about 7 h after separation, the high-gain antenna should be deployed, providing both uplink reception and medium- or high-rate telemetry downlinking for the rest of the TTP (and mission).

3. **Halo Orbit Phase (HOP)**: it starts at the spacecraft's injection into the halo orbit. The subphases of the HOP are:
   - Commissioning Subphase: This phase starts with injection into the halo orbit and ends after successful check-out and commissioning for all on-board instruments. It may last up to one month.
   - Mission Operations Subphase: it includes all scientific and routine operations necessary to undertake the desired experiment activities.

   During this phase, the satellite will be three-axis-stabilised in a Sun-pointing attitude. In the case of safe-mode activation, it maintains this Sun-pointing attitude but to a lower accuracy.

1.4 Phases-ConOps correlation

The sequential relationship of the identified functions and their correlation with the mission phases is fixed by placing them on a timeline, that outlines the logic flow of the conceptual operations of the 2-years nominal mission. [64]

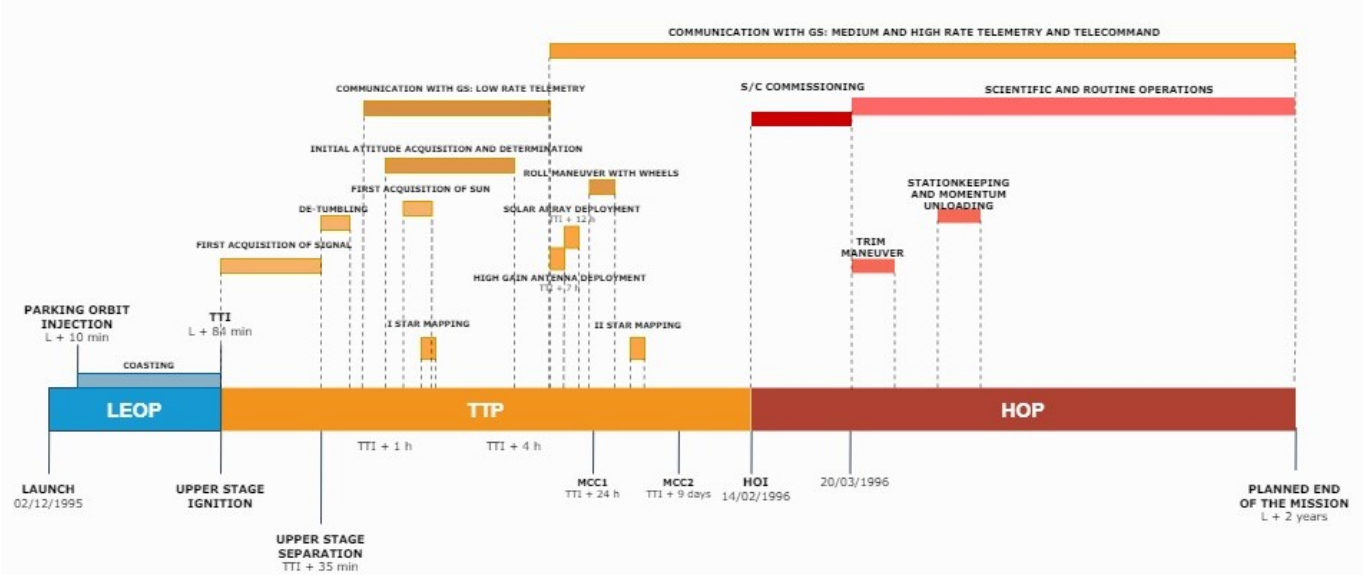

Fig. 2: SOHO Conceptual Operations

1.5 Scientific instruments

1.5.1 Payloads overview

As per one of the major requirements, the spacecraft is divided into two main elements: the Service Module (SVM) and the Payload Module (PLM).
The payload module housed the payloads, fully comprised of scientific instruments aimed at fulfilling the main objectives outlined in Tab. 2. To achieve these goals SOHO carries 12 payloads conceptually divided into three segments [48]:

Helioseismology payloads: high-precision measurements of solar oscillations are easily provided by three helioseismology instruments.

- **GOLF**: GOLF studies the internal structure of the Sun by measuring velocity oscillations over the entire solar disc. It uses a very stable sodium-vapour resonance scattering spectrometer to observe low-degree oscillation modes of the global solar velocity field. It also measures the long-term variations in the global average of the magnetic field;
- **MDI/SOI**: MDI records the vertical motion ("tides") of the Sun's surface at a million different points for each minute. By measuring the acoustic waves inside the Sun as they perturb the photosphere, scientists can study the structure and dynamics of the Sun's interior. MDI also measures the longitudinal component of the Sun's magnetic field;
- **VIRGO**: VIRGO characterises solar intensity oscillations and measures the total solar irradiance (known as the 'solar constant') using two different types of absolute radiometers;

Coronal payloads: the study of dynamic phenomena, taking place in the chromosphere, will focus on plasma by realizing spectroscopic measurements and high-resolution images. The plasma analysis will provide temperature, density and velocity measurements of the outer solar atmosphere material.

- **CDS**: CDS detects emission lines from ions and atoms in the solar corona and transition region, providing diagnostic information on the solar atmosphere, especially of the plasma in the temperature range from 10 000 °C to more than 1 000 000 °C. It is equipped with both a normal-incidence and a grazing-incidence spectrometer, and it uses its measurements to determine the temperatures and densities of various coronal structures;
- **EIT**: EIT provides full disc images of the Sun at four selected colors in the extreme ultraviolet corresponding to four different temperature regimes. It thus provides the morphological context for the spectral observations to be made by SUMER and CDS;
- **LASCO**: LASCO observes the outer solar atmosphere, the corona. It consists in a triple coronagraph with concentric annular fields of view with progressively larger included angles. It is the first spaceborne mirror coronagraph;
- **SUMER**: SUMER is used to perform detailed spectroscopic plasma diagnostics (flows, temperature, density, and wave motions) of the solar atmosphere, from the chromosphere through the transition region to the inner corona. It consists in an UV telescope equipped with a normal-incidence spectrometer;
- **UVCS**: UVCS blocks the bright light from the solar disc and allows observation of the less intense emission from the extended corona. It is an occulted telescope equipped with high-resolution spectrometers in order to locate and characterise the coronal source regions of the solar wind, to identify and understand the dominant physical processes that accelerate it, and to understand how the coronal plasma is heated;
- **SWAN**: SWAN is the only remote sensing instrument on SOHO that does not look at the Sun. It watches the rest of the sky, measuring hydrogen that is 'blowing' into the Solar System from interstellar space. By studying the interaction between the solar wind and this hydrogen gas, SWAN determines how the solar wind is distributed. As such, it can be qualified as SOHO's solar wind 'mapper'. Therefore SWAN will provide the density of the outer most corona.;

Solar-wind and **particle** payloads: measuring the ionic charge states and velocity distributions of ions originating in the solar atmosphere, the energetic particles 'in-situ' and the elemental and isotopic abundances will be the main purpose of solar wind and particle payloads.

- **CELIAS**: CELIAS continuously samples the solar wind and energetic ions of solar, interplanetary and interstellar origin, as they sweep past SOHO. It analyses the density and composition of particles present in this solar wind and it warns of incoming solar storms that could damage satellites in Earth orbit. It measures the mass, ionic charge and energy of the low-and high-speed solar wind, of suprathermal ions, and of low-energy flare particles. It consists of three mass- and charge- discriminating sensors based on the time-of-flight technique, making use of electrostatic deflection, post-acceleration and residual-energy measurements;
- **COSTEP**: COSTEP detects and classifies very energetic particle populations of solar, interplanetary, and galactic origin. It helps to study energy-release and particle-acceleration processes in the solar

atmosphere, as well as particle propagation in the interplanetary medium. It measures the energy spectra of electrons (up to 5 MeV), protons and He nuclei;

- **ERNE**: ERNE measures high-energy particles originating from the Sun and the Milky Way. It measures the energy spectra of elements in the range Z(Atomic number) = 1-30 and abundance ratios of isotopes. It is a complementary instrument to COSTEP;

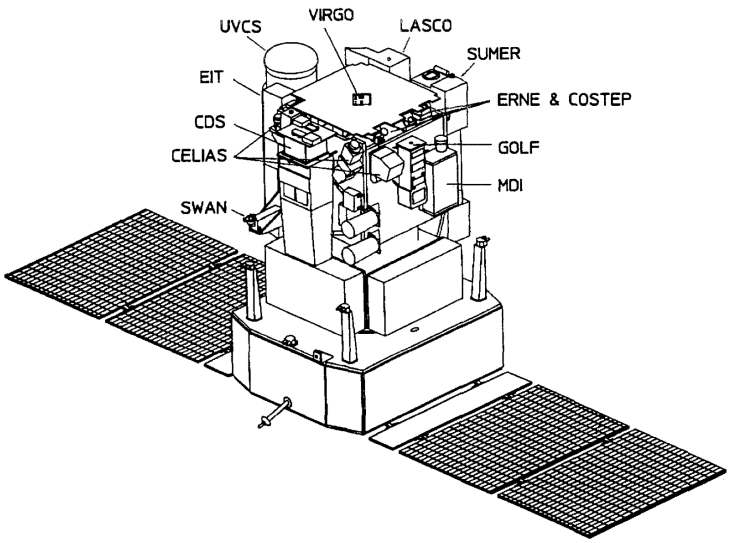

Fig. 3: SOHO spacecraft schematic view with payloads [**?**]

1.5.2 Goals - Payloads correlation

The segments division proposed before reflects the high-level goals of the mission, in particular:

Mission goals	**Payloads**
Probe the internal structure of the Sun	GOLF - MDI - SOI - VIRGO
Characterise the strong and weak magnetic-field regions in the Sun's chromosphere and corona	CDS - EIT - LASCO - SUMER - UVCS - SWAN
Investigate the outflow of solar plasma and detailing the origin of the solar wind	CELIAS - COSTEP - ERNE
Improve the prediction of climate and natural hazards, playing a lead role in the early warning system for space weather and evaluate the Sun impact over climate change	VIRGO - UVCS - CELIAS - COSTEP - ERNE

Table 3: Goals - Payloads mapping

1.5.3 Payloads - ConOps/Phases correlation

To ensure the effective integration of payloads, it's crucial to correlate them with the ConOps and mission phases, thereby optimizing their utilization and management.
The table shown in Fig. 4 presents the various activities of each payload and how they develop in time.

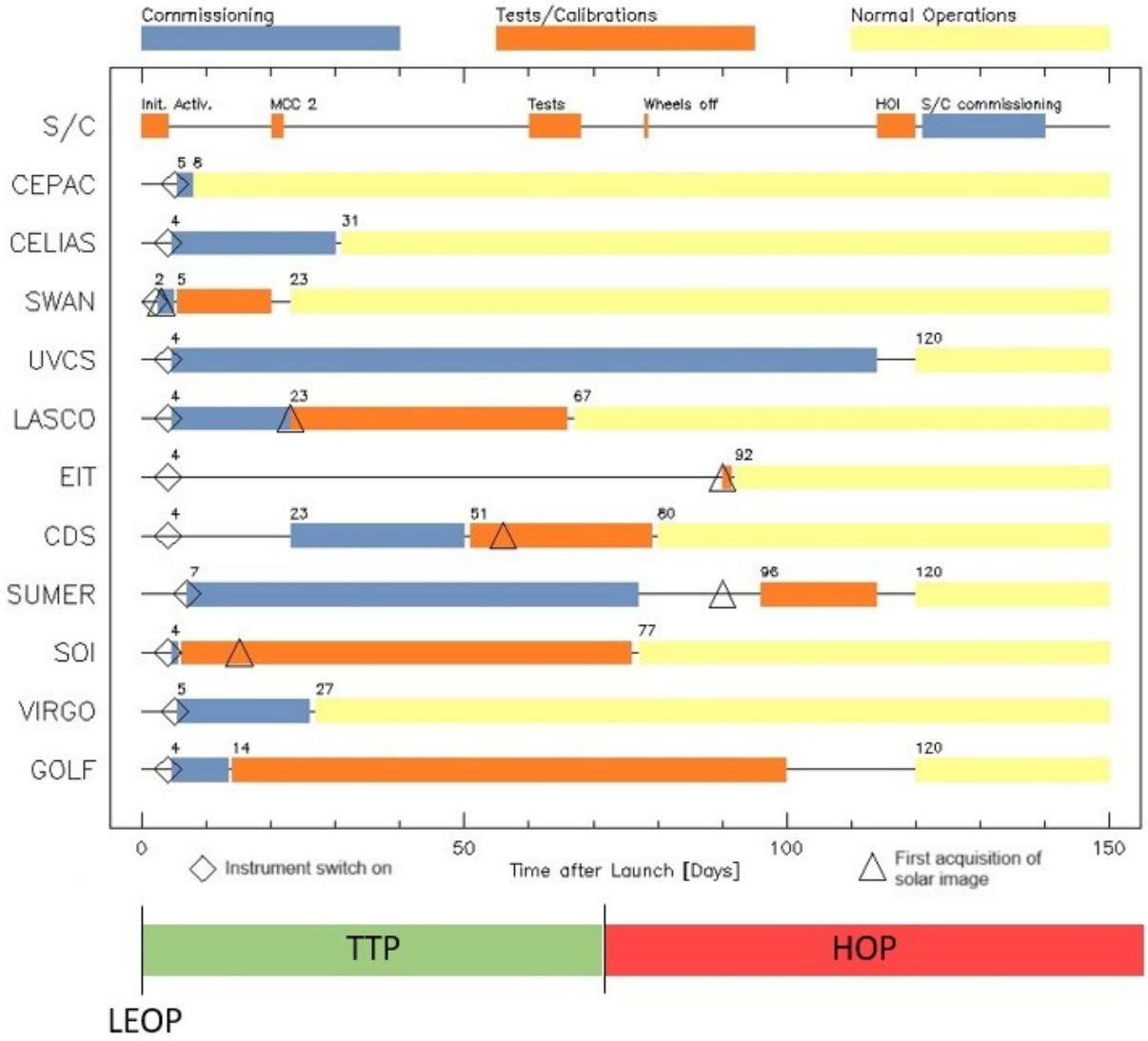

Fig. 4: Payloads - Phases correlation [65]

1.6 Mission Analysis [44] [46] [64] [47]

1.6.1 Mission Requirements and Orbit

The scientific instruments chosen to fulfill the mission goals induce the design of the orbit. In order to provide the best measurements the payloads need:

- Uninterrupted observation of the Sun, without periodic interruptions due to Earth eclipses;
- Smooth Sun-spacecraft velocity changes throughout the orbit, which is required to obtain accurate helioseismology measurements;
- Be permanently outside the magnetosphere, which is appropriate for the 'in-situ' sampling of the solar wind and particles;
- Good position for communication with Earth at all times, necessary by the high rate of real-time science commanding and a large amount of real-time contact required for the mission;
- To navigate around the edge of the Solar Exclusion Zone without entering it directly, to avoid solar interference with communications.

1.6.2 Trajectory Design and Phases

- **Launch and Early Orbit Phase**: SOHO was launched by the Atlas-IIAS using a Centaur upper stage, from Kennedy Space Center. In this phase, SOHO/Centaur is injected into a nearly circular parking orbit, at 150-200 km altitude and inclined at 128.5°. The orbital period is 90 min.

- **Transfer Trajectory Phase**: In this phase the Centaur upper stage ignited at the Transfer Trajectory Insertion (TTI) point, placing SOHO on a direct transfer trajectory to the Sun-(Earth-Moon Barycenter) libration point L1 and its Halo Orbit Insertion (HOI) point at 1.5×10^6 km sunward from the Earth, where the balance of the Sun's gravity and the Earth's gravity is equal to the centripetal force needed for an object to have the same orbital period in its orbit around the Sun as the Earth.
- **Halo-Orbit Phase** The halo orbit is centered in the $L1$ point and lies in the constantly moving plane, which passes through L1 and is perpendicular to the line connecting the Sun and the Earth. The SEV specification constrains the Sun-Earth-Vehicle angle never to be less than 4.5°, while the gimble rate of the High Rate Antenna and the transfer trajectory limit the Sun-Earth-Vehicle angle never to be greater than 32 degrees.

Perigee Altitude [km]	Apogee Altitude [km]	Period [days]	SEV angle [deg]
206 4488	668 672	178	4.5 to 25.5

Table 4: Halo orbit features [47]

The orbit and distance involved in the halo orbit present some operational challenges, indeed there will be a 5 s (approx.) light time delay in communications each way to SOHO, which makes it difficult to perform command verification.

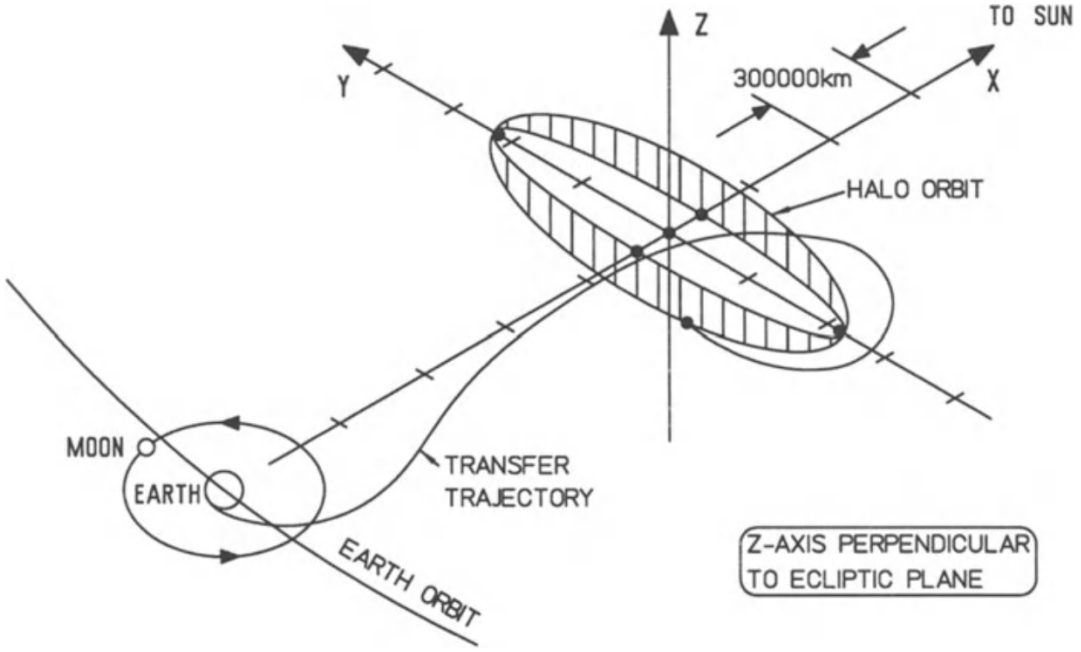

Fig. 5: SOHO trajectory

Change log	
Paragraph number	Brief description of changes
2	pp. 14: Added reference in Table 5.
2.1.2	pp. 15: further explanation of the model and of the results. Correction of data and results.
2.2	pp. 16: change of adopted margins and better specification of the used jets.
3.1	pp. 16: added reference
3.2	pp. 17: rearrangement and further explanation of propellant selection
3.2	pp. 18-19: Correction of data in table 9. Further analysis on tank's material and shape. Correction of results. Better specifications about adopted margins. Further comments on the obtained results, in particular about blowdown ratio, mass of the tank and total mass. Better justification of the choice of pressurizer.
3.3	pp. 19-20: Added explanation on the position of the tank. Further specifications about thrusters configuration.
3.4	pp. 20: modified and further justified power budget

2 Mission Analysis

SOHO is situated in a halo orbit around the Sun-Earth libration point L1 at 1 500 000 km from the Earth with a period of 178 d.

Functionalities	Orbit goals	Orbit Features [47]
Uninterrupted observation of the Sun	No Earth eclipses	$A_x = 206\,448$ km
Helioseismology measurement	Smooth Sun-S/C velocity changes	$A_y = 666\,672$ km
Be outside the magnetosphere	Correct sampling of solar wind	$A_z = 120\,000$ km
Good communication with Earth	Manage science data without interference	SEV angle: 4.5° to 25.5°

Table 5: Functionalities and Halo orbit

2.1 Trajectory design and Costs

2.1.1 Transfer Trajctory

Nominal Orbital Maneuvers [71] During the Launch and Early Orbit Phase (LEOP), the Centaur upper stage injects SOHO into the transfer orbit for the L1 point, the corresponding time of flight is about 4 months. After that, the mission enters the Transfer Trajectory Phase (TTP) and 2 Mid-course correction maneuvers are planned:

- **First Mid-course correction (MCC1)**: divided in a $4.66\,\mathrm{m\,s^{-1}}$ maneuver in the x-direction using thrusters and 1 and 2, and a $0.34\,\mathrm{m\,s^{-1}}$ maneuver in the z-direction using thrusters 7 and 8.
- **Second Mid-course correction (MCC2)**: performed in three segments, one segment of $6\,\mathrm{m\,s^{-1}}$ in x-direction and two segments of $15.7\,\mathrm{m\,s^{-1}}$ and $10\,\mathrm{m\,s^{-1}}$ in the z-direction.

The MCC2 is performed to optimize the Halo Orbit Insertion (HOI) maneuver, which is characterized by a delta-V of $14\,\mathrm{m\,s^{-1}}$ in the x-direction. The HOI is followed by a $0.89\,\mathrm{m\,s^{-1}}$ trim maneuver.

Simplified transfer trajectory model A simplified counter-calculation of the HOI maneuver has been computed by making the following assumptions:

- Transfer trajectory as a single Lambert arc between Earth and L1;
- Circular motion of the heliocentric L1 orbit.

Exploiting the already implemented `LambertMR.m` function, a ΔV of $472\,\mathrm{m\,s^{-1}}$ has been found. It's immediate to notice the discrepancy concerning the real data but remains reasonable given the assumptions under which it has been calculated. Numerical results coming from an analysis available in the literature, concerning the transfer trajectories from Earth parking orbits to Sun-Earth Halo orbits, showed that there are specific locations in the halo orbit where it is reasonable to expect that a transfer can be accomplished for relatively low insertion cost, in particular, halo orbit insertion maneuvers near the 'halo apogee' may be smaller than those near 'halo perigee'.

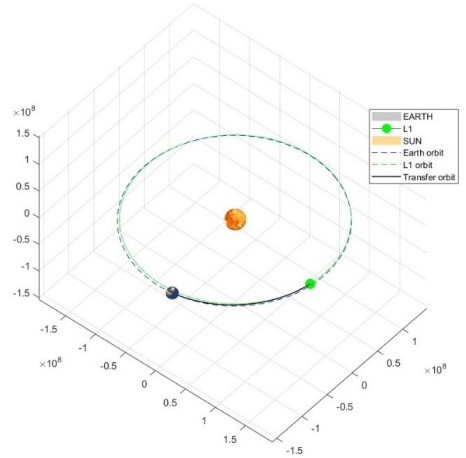

Fig. 6: Transfer arc

This explains the difference in the maneuver cost obtained through the Lambert algorithm, particularly by targeting L1 as arrival point, instead of a specific point on the halo orbit itself.

Comparison with ISEE-3 mission The aforementioned study [52] analyzed the HOI cost especially for ISEE-3 in the function of the time of flight and the amplitude in the z-axis. The ΔV for a transfer with the SOHO characteristics (5) is $32.33\,\mathrm{m\,s^{-1}}$. This value doubles the SOHO's, probably because the study doesn't include the mid-course correction maneuvers; in particular, the SOHO's MCC2 aim is to optimize

the HOI. However, the total cost of the SOHO's TTP (including both the MCCs) is $51.59\,\mathrm{m\,s^{-1}}$ which is comparable with the ISEE-3.

SOHO transfer	Simplified Transfer	ISEE-3 transfer
$51.59\,\mathrm{m\,s^{-1}}$	$472\,\mathrm{m\,s^{-1}}$	$32.33\,\mathrm{m\,s^{-1}}$

Table 6: Final Comparison

2.1.2 Station keeping maneuvers

Nominal Station keeping After the HOI, the mission enters the Halo Orbit Phase, characterized by the Halo Orbit's maintenance. The basic SOHO station-keeping strategy is based on an orbital energy balancing technique, where the entire ΔV is applied along one specified axis. In the nominal design, emphasis is placed on maximizing time-of-flight between maneuvers in order to minimize interruptions in the science observation. So the time between maneuvers would be above 100 d, which would lead to three station-keeping actions per year. Assuming the extended nominal life of six years for the mission and the cost for a single maneuver of 1.89 m/s, which is the maximum delta-V registered in the nominal condition [**?**], the total cost of the station-keeping is 34.02 m/s.

Simplified solar radiation pressure model The prevalent external disturbance acting on spacecrafts in halo orbit is the torque due to solar radiation pressure. A simple model has been computed to have an estimation of the SRP's effect on SOHO. The following assumptions were made:

- SOHO's orbit around L1 is considered circular with the amplitude specified in Table 5
- SOHO is modeled as a parallelepiped to compute the Inertia moment;
- No value of angular velocity was found, so the ISEE-3's angular speed is utilized: [2.0944; 0; 0] rad/s [52];
- Reflectance factor: $\rho = 0.5$ [52];
- SRP torque: $T_{SRP} = \frac{F_s}{c} A(1+q)(CM-CP)$ where F_s is computed with the formula found in literature [38];

By applying the Euler equation and integrating the angular acceleration, the angular velocity is obtained; after that the ΔV is recovered by considering the equation $I\omega = mrv$ where r is the distance between the spacecraft and L1 point and v is the velocity vector around the three axis, the shift to which SOHO is subjected after one year is computed.

Solar Power density at L1 (F_s)	$1411\,\mathrm{W/m^2}$
Area of the SOHO surface exposed to the Sun with solar panels	3.7 m * 9.5 m = 35.15 $\mathrm{m^2}$ [44]
Center of mass and center of pressure offset	[0.07; 0.07; 0.07]m [59]
SRP torque	[1.7374; 1.7374; 1.7374] $\cdot 10^{-5}\,\mathrm{N\,m}$
Inertia moment with solar panels	diag[3.7577; 4.9161; 4.4231]$\cdot 10^3$ $\mathrm{kgm^2}$
SOHO shift without SRP	[0.6453; 0; 0]m
SOHO shift with SRP	$[0.6902;\ 8.357 \cdot 10^{-10};\ -7.273 \cdot 10^{-9}]$m
SOHO net shift	$[0.045;\ 8.357 \cdot 10^{-10};\ -7.273 \cdot 10^{-9}]$m

Table 7: SRP model results

The results show that the SRP torque causes a little offset on SOHO and the correcting delta-V needed is undeniably smaller than the one assumed before. This is probably because other perturbances are acting on SOHO, as the internal perturbances caused by the thruster misalignment, that are not taken into account, but that could be significantly higher than the SRP. Although this computation is only a simplified way to compute the effects of the external disturbances on the SOHO attitude, the results show that station-keeping manuevers are needed throughout the all the mission to control the spacecraft.

2.2 ΔV budget breakdown

Phase	Maneuver	ΔV $[m/s]$	Jets	Margin
TTP	MCC1	4.66	1-2	5%
		0.34	7-8	
	MCC2	6.00	1-2	5%
		15.70	7-8	
		10.00	7-8	
	HOI	14.00	/	5%
		0.89	1-2	
HOP	SK	34.02	1-2 / 3-4	100%
Total ΔV with margins		122.21 m/s		

Table 8: ΔV breakdown [71][73]

The MCC1, MCC2 and HOI costs [71] are deterministic chemical propulsive maneuvers and their relative margin is set at 5% of the maneuver cost [39], instead the station keeping delta-V is not analytically derived so the margin assumed is 100% [39]. Then the total cost is obtained by summing all the maneuvers costs with their respective margins. In the literature, the total ΔV capability of SOHO is stated as around 318 m/s though only 275 m/s of that is allocated to the overall delta-V budget, and the remainder is reserved for attitude control including momentum management maneuvers. This value is higher compared to the delta-V computed in Tab. 8, the reasons can be improving the reliability of the satellite and keeping the possibility to extend even further the mission's lifetime.

2.2.1 Mission Anomalies

During its operation, the SOHO mission encountered two mission-threatening anomalies:

- The first anomaly involved the complete loss of communications for several weeks.
- The second anomaly involved the loss of gyroscopes coupled with the loss of normal attitude control.

In order to restore the mission to full working condition different maneuvers were performed, and the total cost is $31.53\,\mathrm{m\,s^{-1}}$[73]. As we have seen before the spacecraft had enough ΔV capability to perform the recovery burns without compromising on the mission objectives. However, a new design of the station-keeping maneuvers was required in order to compensate for the loss of the gyroscopes. The new design implements a fixed 90-day cadence SK maneuver, which has resulted in an overall lowering of annual station-keeping costs.

3 Propulsion System

3.1 Mission propulsion architecture

The SOHO spacecraft is equipped with a total of sixteen Northrop Grumman's monopropellant hydrazine thrusters (MRE-1.0) [20]. Each of them weights 0.5 kg, measures 190 mm in width and 39 mm in length, provides 220 s of specific impulse and 3.5 N to 5 N thrust. They are fundamentally divided into two branches of eight thrusters each (the so called dual thruster modules DTM); four of them (DTM 5 to 8) are located on masts mounted on the upper platform of the service module (SVM), two of them (DTM 1 and 2) on the upper platform and the last two (DTM 3 and 4) are located on the bottom side of the spacecraft.
The SOHO spacecraft propulsion system is powered by pressurized hydrazine (N_2H_4), confined in a prolate spheroidal tank, with a specified gas mass (GHe); therefore operating in a blow-down mode. This mode avoids the need for additional gas pressurant vessels thereby reducing mass, volume and propulsion systems complexity.
The thrust generation process develops according to the following phases:

- First, the attitude-control system signal leads to the opening of a fill and drain valve that loads and drain the propellant, allowing hydrazine to flow properly in the system, while expelling the unwanted air. This action may be pulsed (as short as 5 m sec) or long duration (steady state). Moreover, the pressure transducer measures the internal pressure of the tank and regulates, throught the valves, either insertion or removal of hydrazine into the system.
- The pressure in the propellant tank forces liquid hydrazine into the injector. It enters as a spray into the thrust chamber and contacts the catalyst beds (alumina pellets impregnated with iridium).

During the fuel injection process, the latch valve provides a fully reliable safety barrier in propellant flow lines between propellant tanks and thrusters. The valve is equipped with a back relief function that protects the downstream lines and equipment against over-pressure (e.g. due to environmental effects).

- Once the liquid hydrazine remains in contact with the catalyst bed, the vaporizing point is reached. The temperature of the hydrazine rises to a point where the rate of its decomposition becomes extremely high and the chemical reactions become self-sustaining.
- Finally, inside the space thrusters, the hydrazine decomposition products leave the catalyst bed, exit from the chamber through a high expansion ratio exhaust nozzle and produce the desired thrust value.

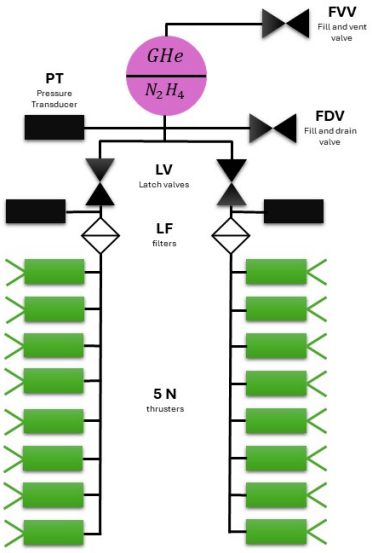

Fig. 7: Propulsion architecture [44]

3.2 Propellant selection and tank sizing

The propulsion system chosen for the SOHO mission was hydrazine monopropellant. This decision was based on several factors. [54] Firstly, the propulsion system needed to provide the necessary delta-v for both the transfer trajectory phase and station-keeping maneuvers. Hydrazine monopropellant is suitable for these requirements due to its ability to modulate thrust and perform precise maneuvers.
The simplicity and reliability of the propulsion system, paired with propellant storability, minimize the system's failure potential during the operational lifetime. Moreover since SOHO contains optical instruments like star trackers or cameras, it was required to avoid that contaminants derived from the propellant plume deposit on optical surfaces to ensure the maximum performances of the instruments, monopropellant hydrazine reaction gases satisfy greatly this requirement.
In contrast, solid propellant was excluded due to its inability to modulate thrust and its lack of reusability, and as for bipropellant systems due to their complexity and storability issues.
Electric propulsion was also discarded because of its architectural complexity and the lower technology maturity, even if it could have potentially brought propellant mass savings. Additionally, the possibility of electromagnetic interference from the power conditioner and thruster posed risks to the payload's electromagnetic measurements.

Moreover, at the time of the mission's design, hydrazine monopropellant systems had a much higher Technology Readiness Level (TRL) compared to electric and nuclear propulsion systems, further reducing the risk of failures.

The sizing of the propulsion system of the SOHO satellite has been performed considering the actual ΔV budget since the results obtained with the approximated analysis were considered too far from the real ones. Here are presented data and assumptions made for the dimensioning:

Reference data		
Specific Impulse [20]	I_{sp}	220 s
Initial Mass [44]	M_0	1863 kg
Total velocity budget [73]	ΔV_{tot}	318 m/s
Initial tank pressure [73]	$P_{tank,i}$	22.4 bar
Final tank pressure [73]	$P_{tank,f}$	6.6 bar
Thruster mass [20]	m_{thrust}	0.5 kg
Assumptions		
Tank temperature [39]	T_{tank}	293.15 K
Ti6A14V Tank density [58]	ρ	4430 kg/m^3
Ti6A14V Tank strength [58]	σ	950 MPa

Table 9: Mission PS Data [72][20]

The initial tank temperature is chosen in compliance with propellant temperature requirements. The most common tank material for blow-down monopropellant hydrazine is Ti6A14V. It provides an high ultimate tensile strength and it is compatible with the propellant which is instead corrosive with aluminum and steel. Moreover it is resistant to high temperatures without significant deformation or loss of mechanical properties.

In this design, appropriate margin are considered as stated in reference [39].

Starting from the ΔV budget, a 5% margin is added as the starting value were obtained from deterministic, calculated manoeuvres. So the mass ratio MR thus can be immediately computed as:

$$MR = \frac{M_0}{M_f} = e^{\frac{\Delta V_{real}}{I_{sp} g_0}} = 1.167 \rightarrow M_f = \frac{M_0}{MR} = 1596.0\,\text{kg} \tag{1}$$

To get the total dry mass at launch it was established a proper system level mass margin of 20%:

$$m_{dry} = \frac{M_f}{1.2} = 1330\,\text{kg} \tag{2}$$

Then, it follows that the propellant mass is:

$$m_{prop} = (M_0 - M_f) \cdot margin_{prop,m} = 281.7\,\text{kg} \tag{3}$$

Where $margin_{prop,m} = 1.055$, consisting in an additional 3% due to ullage , 2% of residuals and 0.5% of loading uncertainty.
Knowing the density of the hydrazine propellant, the occupied volume is calculated:

$$V_{prop} = \frac{m_{prop,real}}{\rho_{N_2H_4}} \cdot margin_{prop,V} = 0.309\,\text{m}^3$$

where $margin_{prop,V} = 1.10$ is considered to take into account unusable volume (10 %).

Afterwards, considering that the satellite is equipped with a blow-down pressurization system, it becomes necessary to define the blow-down ratio. Starting from the initial and final pressure reported in 9, the Blow-down ratio is determined as:

$$B = \frac{P_{gas,i}}{P_{gas,f}} = 3.39 \tag{4}$$

Typical blow-down ratio for analogous applications are in the range between 4 and 6, while the one obtained is slightly lower. This influences the overall mass of the propulsion system, increasing both the pressurizing gas and tank mass. However this increase is limited (B=4 saves only 0.5kg (3%) of the propulsion system mass). On the other hand, this value increases the subsystem reliability, considering a margin from the maximum and minimum operating pressure of the engine [20].

Once the Blow-Down ratio is known, it is applied isothermal to compute the initial pressurizing gas volume:

$$V_{gas,i} = \frac{V_{prop,real}}{B-1} = 0.129\,\mathrm{m}^3; \tag{5}$$

The isothermal model is a close representation of the slow flow blow-down process.

Then the mass of the pressurizing gas is evaluated using the perfect gas law, assuming the initial tank temperature of 293.15 K. The choice of the pressurizing gas fell on Helium that, being a noble gas, is lighter, non-flammable and less reactive than Nitrogen. Furthermore, choosing Helium allows for a 85.7% savings on the mass of the pressurizing gas that needs to be used, leading to a reduction in volumes and costs. As suggested for pressure-fed systems an additional 20% margin on the mass is considered:

$$m_{press} = \frac{P_{tank,i} V_{gas,i}}{R_{He} T_{tank}} \cdot margin_{press} = 0.568\,\mathrm{kg}; \tag{6}$$

Then, the tank is determined knowing the pressurizing gas initial volume, the propellant initial volume and by adding a 1% due to bladder volume:

$$V_{tank} = (V_{prop} + V_{gas,i}) \cdot margin_{tank,V} = 0.442\,\mathrm{m}^3 \tag{7}$$

As preliminary design it is assumed a spherical tank shape, the radius is obtained as:

$$r_{tank} = \left(\frac{3V_{tank}}{4\pi}\right)^{1/3} = 0.473\,\mathrm{m} \tag{8}$$

Knowing the material strength, the tank thickness of the tank is computed as:

$$t_{tank} = \frac{P_{tank} r_{tank}}{2\sigma} = 0.56\,\mathrm{mm} \tag{9}$$

Finally the tank mass is:

$$m_{tank} = \rho_{tank} \frac{4}{3}\pi\left((r_{tank} + t_{tank})^3 - r_{tank}^3\right) = 6.91\,\mathrm{kg} \tag{10}$$

This value is much lower than the one provided by the manufacturing company (34.5 kg, [61]).This is due to a different shape of the tank (Long Oblate spheroid), with the assumed spherical geometry being the most efficient in terms of tank mass. Furthermore both the real tank material and safety factor are unknown, with the latter most likely being higher improving reliability (but requiring an higher mass).

The mass budget of a monopropellant system is defined as the sum of the tank mass, the pressurizing gas and the thrusters mass. To take into account cables also a 10% margin is added:

$$m_{PS} = (m_{tank} + m_{press} + 16 \cdot m_{thruster}) margin_{mass,cables} = 17.02\,\mathrm{kg} \tag{11}$$

The obtained total propulsion system mass is really low, but still a reliable starting point. A crucial trade-off should be considered between occupied space and mass. More accurate estimation would be possible considering the available volume and therefore the real shape of the subsystem.

3.3 Configuration of thrusters and hydrazine tank

The prolate spheroidal tank, containing pressurized hydrazine (N_2H_4) and Helium gas (GHe), previously dimensioned, it is located in the middle of central cylinder of the spacecraft SVM guaranteeing continuous balance around the CoM in case of sloshing due to vibrations. This configuration also allows the CoM to move only along the $+X$ direction, while tank level decreases. Furthermore, the tank is placed in a strategical position to defend the electronics from radiation keeping warm the propellant at the same time.

The total sixteen thrusters are arranged into two fully redundant branches of 8 thrusters, each providing both delta-V during the transfer orbit and station keeping in the L1 point, taking care of primary and secondary propulsion as needed. The primary branch (A-branch) is used for command maneuvers, roll, yaw and pitch attitude control, while the redundant branch (B-branch) is used mainly in an emergency fail-safe

mode. This dual-branch configuration enhances redundancy and reliability in both propulsion and control systems.

Thrusters Pair	Thrusters Locations	ΔV direction (body frame)	Primary attitude control
1 and 2 (1 is canted 30° down; 2 at 30° up)	Fore (Sunward)	$-X_B$	Pitch
3 and 4	Aft (Earthward)	X_B	Yaw
5 and 6	Top ($+Z_B$)	$-Z_B$	Roll
7 and 8	Bottom ($-Z_B$)	Z_B	Roll

Table 10: Thrusters configuration data [57]

In particular, thrusters 1 and 2, are canted 30° out to minimize plume impingement on the payload module, since $+X_B$ direction is that along which the instrument bore-sights are intended to point at the Sun. This is crucial for the integrity of scientific data collection onboard.

The inclined thrusters (DTM 1 and 2) are partially sun illuminated, DTM 3 and 4 are always in the shadow of the spacecraft and DTM 5 to 8 are exposed to the sun. All nominal thrust components are in the body XZ plane. Given SOHO's solar-pointing attitude, thruster configurations perfectly dovetail with the single-axis control technique, implying that all station-keeping delta-Vs will be parallel (anti-parallel) to the SOHO Sun-line.

3.4 Power budget

The preliminary power budget for the propulsion subsystem is computed starting from the nominal power needed for one thruster, 8.5 W [20]. 4 is the number of thrusters considered to be fired simultaneously, since it's the minimum amount needed to control the spacecraft around all his three axis. This results in an overestimation because during maneuvers only two thrusters are usually used at the same time, as stated in Table 8. The utilized thrusters were also adopted in other missions and since they were used without any modifications for the SOHO one, the design maturity power margin was chosen as 5% [20][39].

Thruster Power [W]	Firing Thruster	Total Power [W]	Total Margined [W]	% of total Budget
8.5	4	34	35.7	2.38

Table 11: Power Budget

Where the total power available considered is 1500 W [35], the percentage of power consumed by the propulsion subsystem is in compliance with similar satellite applications which usually address a power budget from 2 % to 10 %. [39]

Change log	
Paragraph number	Brief description of changes
4.1	pp. 22: rearrangement and extended description of TMTC architecture
4.2	pp. 22: rearrangement and extended explanation of frequency selection
4.3	pp. 22-23: reduction of TTP and Normal mode paragraphs
4.5	pp. 23-24: modified description of Ground stations and modified caption of table 12
4.6	pp. 24: correction of encoding strategy and real data rate value
4.6.1	pp. 24: correction of the output power value
4.6.2	pp. 24: correction of Data volume value
4.6.3	pp. 24-25: specification of the used frequencies and rearrangement of table 13
4.6.4	pp. 25: rearrangement of the paragraph, modified value of pointing accuracy and correction of pointing losses values in table 14.
4.6.5	pp. 25: correction of minimum link budget values and values in table 15, in light of the change of the encoding strategy.
4.6.6	pp. 26: correction of SNR values and better specification of roll of factor.
4.6.7	pp. 26: Added paragraph about the LGA with related calculations
4.7	pp. 26: Added SSA mass in the mass budget

4 TTMTC

4.1 TMTC architecture

The ground to satellite links are provided throughout the whole mission by an S-band Radio Frequency (RF) system (2245 MHz and 2067 MHz for down- and up-link, respectively). The transmission of telemetry data to ground, telecommand reception and tracking/ranging functions are conducted via NASA's Deep Space Network (DSN). With the objective to meet all its specific requirements, the TTMTC subsystem's architecture comprises:

HGA: one directional 804 mm S-band shallow parabolic reflector high gain antenna, integrated in the spacecraft central tube. The HGA requires direct pointing of ground stations and is used during the operational phase of the SOHO mission. During this time, the spacecraft will be on it's orbit around L1 and pointed towards the Sun along the $+X$ direction. To maintain pointing the HGA was therefore located on the face pointing towards Earth in the $-X$ direction.

LGAs: two low gain antennas that are meant to maintain omni-coverage so as to always be able to transmit telemetry data (but usable only with low rate telemetry), even during phases in which precise pointing is not possible (for example during detumbling): for this reason they are mounted on opposite sides of the spacecraft. They are indeed installed on the $+Z$ and $-Z$ side of the spacecraft[**?**], mounted on fixed booms at the bottom section of the service module protruding from the main body to provide full geometrical coverage and to minimize interference with the on-board electronics. They are quadrifilar short resonant helix antennas with a wider beamwidth than HGA. The antenna pattern is quasi-rotationally symmetric and quasi isotropic in the region of elevation between 0 and 108.50 deg (LGA reference axis).

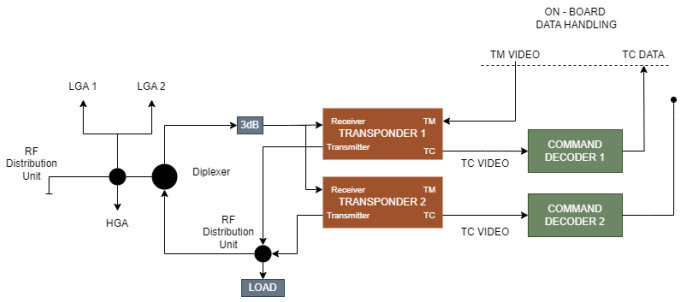

Fig. 8: TMTC architecture

The system is completed by a set of:

Thomson-CSF transponders (S-band): the TTC transponder transmits the telemetry data, receives the telecommand signals, demodulates the ranging tones and re-transmits them to ground.[43]

HPA: high power solid-state amplifier that provides 10 W and 3.2 W output levels in its high and low power mode respectively, in order to allow data transfer through the antenna. This kind of amplifier may be preferable over Travelling Wave Tube Amplifier (TWTA) because of the reduced weight and the sufficient output power. In fact for applications that requires less than 10 W a SS amplifier is generally preferred. [39]

4.2 Frequency selection

The S-band frequencies, typically ranging from 2 GHz to 4 GHz, are widely used in space communications given the several advantages that they bring with. Regulatory considerations outlined by the ITU annexes [74] also favor S-band frequencies over both X-band and Ku/Ka-bands, especially given the specific requirements and operational conditions of the SOHO mission:

- Thanks to the abundant time windows available for data transmission, lower data rates are sufficient, allowing data rate requirements of the mission to fall within the S-band range;
- S-band offers advantages such as a larger beam width, requiring less precise pointing and enabling faster recovery in case of failure;
- S-band signals penetrate the Earth's atmosphere effectively, maintaining stable and reliable communication links, while higher frequencies, such as those in the X-band, are associated with increased atmospheric losses and tend to to exhibit higher noise levels due to the higher temperatures of the receiver.

4.3 TTMTC - Phases/Ops/Modes correlation

The selection of data-rates, frequencies and band type is associated to the type of data to be transferred to and from the spacecraft at each mission phase:

- **LEOP**: during launch and throughout the coasting phase neither communication with Earth nor acquisition of data is foreseen.
- **TTP**: from the first acquisition of signal right after the injection in the transfer orbit, both low gain antennas ensures low rate telemetry at $1.4\,\mathrm{kbit\,s^{-1}}$. During the TTP, considering the trajectory correction maneuvers, maintaining communication coverage over a broad area is essential, in order to transmit the telemetry data and receive commands. When the spacecraft is approaching its final orbit and settling into its operational scientific phase, also the high gain antenna is deployed, and both medium- and high-rate telemetry is provided respectively at 54.6 kbit/s and 245.8 kbit/s. This allows for faster transmission of scientific data, telemetry, and command signals between the spacecraft and ground stations.
- **HOP**: it is the core of the scientific operations, during which SOHO payload produces a continuous science data stream of $40\,\mathrm{kbit\,s^{-1}}$. The former is increased by $160\,\mathrm{kbit\,s^{-1}}$ whenever the solar oscillations imaging instrument (MDI) is operated in its highrate mode, during the long station pass.

Furthermore the different pointing modes that can be adopted throughout the mission, are decisive in particular with respect to the role of the antennas [66]:

- **Normal mode (NM)**: with full knowledge of SOHO's orientation (coming from the Fine Pointing Sun Sensor (FPSS) and a star tracker) the High Gain Antenna (HGA) can be steered to point at the Earth, providing a High Rate downlink of telemetry using 26-meter ground stations.
  Due to a failure occurred in the HGA Z-axis due to malfunctions in the pointing mechanism, SOHO experiences telemetry 'keyholes' twice per orbit, roughly every 3 months.
  Later using larger 34-meter stations with better receivers instead of the standard 26-meter stations, SOHO managed to keep beaming high rate data through the HGA for a few days extra on each side of the keyhole;
- **Emergency Sun Reacquisition (ESR) Mode**: ESR mode can be triggered by a number of "safety features", such as the FSPAAD, which is supposed to trigger when the Sun is outside a 5-degree radius error circle. In this mode, the High Gain Antenna (HGA) cannot be correctly pointed towards Earth, because spacecraft attitude is performed just approximately. Instead, the omnidirectional Low Gain Antenna (LGA) is used to transmit vital information to ground controllers, at medium rate telemetry with 34-meter ground stations;
- **Coarse Roll Pointing (CRP) mode**: it's the transition mode, while recovering from ESR, in order to retrieve near nominal roll orientation. Finally HGA can be correctly oriented towards Earth.

4.4 Contact strategy

In normal mode 13 hours of daily real-time contact is foreseen[63]:

- 1.6 hour contacts: during which the FOT retrieves the science and housekeeping data which have been recorded onboard during the previous 3.7 hours,and perform any necessary maintenance such as ephemerides updates, instrument and star-tracker table loads, etc. There will also be a brief (5-10 minute) downlink of magnetogram data from MDI;
- 8 hour contact each day: the primary time reserved for real-time science collection.

During periods without DSN contact, SOHO records the housekeeping and science data (equivalent to the 40 kbps telemetry stream) onboard. While in contact with the ground, the nominal mode of operation is high rate telemetry[67].

4.5 Ground stations

The SOHO ground station system constitutes the front-end interface between the operational ground segment and the spacecraft. The whole system development is provided by NASA's Deep Space Network facilities, located in Goldstone, Canberra and Madrid. The complexes are constituted of ultrasensitive receiving and processing systems which include a set of different kinds of antennas, summarized in the table 12 below.

Antenna Type	ID	Site	S-band UF [MHz]	S-band DF [MHz]	Gain [dB]
34m BWG	DSS-26	Goldstone	2025-2110	2200-2300	55,7
	DSS-27				
	DSS-36	Canberra			
34m HEF	DSS-65	Madrid			
70m	DDS-43	Canberra	2110-2120		61,9

Table 12: SOHO DSN Ground stations [6]

Each of them is 120° apart from the other, in order to always provide continuous coverage for the spacecraft. This ensures that at any given time, there is always at least one ground station capable of receiving signals from SOHO, thereby providing uninterrupted data collection and communication with the spacecraft. In the event of gaps in DSN coverage, telemetry-only backup support will be furnished by the Santiago Ground Station (AGO) and the Air Force Satellite Control Network (AFSCN). Before 2009 (that marked the year of their dismantling) also 26-meter antennas were widely adopted since considered to be optimal for the nominal operations (aforementioned Normal Modes (NM) of the SOHO mission), having a maximum tracking speed of three degrees per second, equivalent to tracking one full rotation of an Earth-orbiting spacecraft every two minutes. Some of them were directly dismantled, while others underwent a refurbishment process, transforming into 34-meter HEF antennas, through the replacement of the main dish plate.

4.6 TMTC subsystem sizing

The reverse sizing of the telecommunication subsystem has been performed considering the most demanding mode in terms of available downlink data rate: $40\,\mathrm{kbit\,s^{-1}}$ of science data during scientific operations in HOP, increased by $160\,\mathrm{kbit\,s^{-1}}$ considering MDI in highrate mode, resulting in an overall $245.8\,\mathrm{kbit\,s^{-1}}$ of high-rate telemetry.[44] For the uplink mode instead the data rate considered is the one of the NASA DSN complex which is set as $4\,\mathrm{kbit\,s^{-1}}$.[9] The transponder uses phase modulation in order to increase the data rate and send the same amount of information with less power demand. In the absence of significant data, it is assumed that SOHO uses Bifase Phase Shift Keying (BPSK) because it is the standard for the ESA mission, due to its reliability and less power demand. The encoding strategies used are both R-S(interleaved to a depth of five) and convolutional coding for downlink data.
The real data rate becomes then: $R_{real} = R\,\frac{\alpha_{enc}}{\alpha_{mod}} = 281.07\ \mathrm{kbit\,s^{-1}}$, where $\alpha_{mod} = 1$ and $\alpha_{enc} = 1.1435$, as Reed-Solomon [39] encoding is considered since it normally allows to detect and correct multiple consecutive errors.

4.6.1 Input and Output Power

The output power was chosen from the literature, the one related to the S/C antenna is 10 W [**?**], while the Ground Station antenna emitts 20 kW considering the nominal mode phase with the 26 m diameter antenna. [6] According to the selection made on the solid state amplifier, and giving the output power the input power was computed:

$$P_{input,tx} = \frac{P_{output,tx}}{\mu_{ampl}} = 47.62\,\mathrm{W} \tag{12}$$

where μ_{ampl} is selected from the available chart as 0.21 which is the respective Solid State amplifier gain for an output power of 10 W. [77]

4.6.2 Data Volume

Given the nominal contact time window of 13 hours per day [63], the data volume is easily obtained by multiplying the window with the real data-rate computed in the Section 2: respectively 2.88 MB for a day and 1.05 GB for a year.

4.6.3 High Gain Antenna

The analysis focuses on the sizing of the HGA, which in normal mode is the one that ensures both high rate downlink and uplink of telemetry. The antenna gain depends on the antenna type which is the parabolic one as found in literature. [44] The gain of the antenna has been estimated as follows:

$$G = 10\log_{10}\left(\mu_{par}\left(\frac{\pi\ D}{\lambda}\right)^2\right) \tag{13}$$

where $\lambda = \frac{c}{f}$ is the wavelength taken into account respectively in uplink ($f_{up} = 2067\,\mathrm{MHz}$) and downlink ($f_{down} = 2245\,\mathrm{MHz}$) modes; $\mu_{par} = 0.55$ is the efficiency related to the parabolic shape of the antenna [39]

and $D = 0.804\,\text{m}$ is its diameter. [44]
Analogously, the gain of the ground station antenna can be computed exploiting the previous empirical formula 13, given the antenna dish diameter $D_{GS} = 26\,\text{m}$. Another characteristic parameter for the antennas is their beamwidth, that can be easily evaluated knowing the wavelength of the signal transmitted and the diameter of the receiving antenna:

$$\theta = 65.3 \cdot \frac{\lambda}{D} \tag{14}$$

All the results are here summarized:

	G_{ant}	G_{GS}	θ_{ant}	θ_{GS}
Downlink	22.94 dB	53.13 dB	10.85 deg	0.335 deg
Uplink	22.22 dB	52.42 dB	11.78 deg	0.364 deg

Table 13: Gains and beamwidths

4.6.4 Losses

The losses computation involves four types of contributions: free space, pointing, atmospheric and cable losses have been taken into account. There were considered both uplink and downlink modes. Free space losses and pointing losses have been computed as:

$$L_{free_space} = 20\log_{10}\left(\frac{\lambda}{4\pi r}\right) \qquad L_{pointing} = -12\left(\frac{\eta}{\theta_{rx}}\right)^2 \tag{15}$$

where $r = 1.5 \cdot 10^9$m is the maximum distance of the satellite from the GS, this was assumed with worthy accuracy equal to the distance of L1 point from the Earth surface, η is the relative pointing accuracy assumed as 0.01 deg, for both uplink and downlink, considering the DSN antennas as more precise with respect to other ground station antennas.[39]
Considering that the transmission both in uplink and in downlink occurs using the S-band, atmospheric losses has been estimated as $L_{atm} = -0.04\,\text{dB}$ while the cable ones L_{cab} have been considered equal to $-2\,\text{dB}$ for the spacecraft according with the literature [39], and $-1\,\text{dB}$ for the DSN antennas. The previous equations leads to the following results:

	Downlink	**Uplink**
$L_{free\ space}$	$-223\,\text{dB}$	$-222.3\,\text{dB}$
$L_{pointing}$	-0.0107 dB	-0.000008 dB

Table 14: Losses

4.6.5 Link budget

To compute the link budget, it is necessary to compute the receiver power and the System Noise density both for uplink and downlink.

$$P_{rx} = EIRP + G_{rx} + L_{free\ space} + L_{atm} + L_{pointing} \qquad N_0 = 10\log_{10}(kT_S) \tag{16}$$

where EIRP $= P_{tx} + G_{tx} + L_{cab}$ considering the transmitting antenna; k is the Boltzmann constant and T_S is the antenna temperature, considered as 21 K for the DNS antenna and 250 K for the spacecraft antenna since it is expected to work at higher temperatures. Finally the Error per bit to Noise density is estimated considering the noise on the receiver:

$$\frac{E_b}{N_0} = P_{rx} - N_0 - 10\log_{10}(R_{real}) \tag{17}$$

This result shall be compared with the minimum $\frac{E_b}{N_0}$ chosen considering the right BER (10^{-5} for downlink and 10^{-7} for uplink).[39] For the first case this parameter is usually higher than the second case since commands requires an higher accuracy. By considering the Reed-Solomon encoding strategy, the minimum link budget is estimated as 5.3 dB for downlink and 6.1 dB for uplink. [39]Furthermore a margin of 3 dB is taken into account to verify if the receiver has the capability of distinguish the signal from the noise. The following results satisfy the margins:

	Downlink	**Uplink**
E_b/N_0	21.92 dB	62.35 dB

Table 15: Energy per bit to Noise density

4.6.6 SNR

The computation of the signal to noise ratio requires the selection of a modulation index, since no information are found in literature, this was selected as $\beta = 60\,\text{deg}$ which is the most used value for normal-mode downlink [39]. For the uplink mode the value was taken from [62] as $\beta = 0.8$ rad. Therefore the Carrier power is computed:

$$P_{carrier} = P_{rx} + 20\log_{10}(\cos\beta) \tag{18}$$

The Bandwidth of the signal is computed assuming a mean value (between 0.5 and 1) of the roll-off factor equal to 0.75. From the real data-rate it can be obtained that: $B = R_{data,real}(1 + roll_{off})$, furthermore to compute the Signal to Noise ratio and verify if the receiver has the capability of tracking the signal, distinguished it from the noise. The ground station constraint on the minimum SNR is considered as 10 dB while for the uplink mode the minimum is set as 9.5 dB as similar satellite applications has.[53] The SNR margin, computed as:

$$SNR = P_{carrier} - N_0 + 10\log_{10}(B) - SNR_{minimum} \tag{19}$$

verify the sizing by giving the result of 3.47 dB (downlink) and 47.28 dB(uplink) which is larger than 3 dB margin.

4.6.7 Low Gain Antenna

The two low gain antennas are usable instead only to ensure low rate telemetry at $1.4\,\text{kbit}\,\text{s}^{-1}$, ensuring omni coverage. Their usage is limited to communication with the DSN in the early phases of the mission right after SOHO's separation with the launcher and to emergency mode.
Given the vital role that the LGAs play in ensuring continuous communication even in conditions of coarse pointing accuracy or during de-tumbling, a dedicated sizing is performed.
The dimensioning is performed applying the same encoding strategy of the HGA(R-S) and considering the low data rate telemetry ensured by the low gain antenna.[44]
Since the low gain antenna has a quasi-isotropic behavior in a wide range of the mission, to compute the diameter of the helix antenna the assumption of circumference equal to wavelength has been made.[44] Considering the downlink phase and the corresponding frequency therefore a diameter of 4.25 cm has been found. To proceed with the sizing also the length of the isotropic antenna has to be computed considering the $G_{LGA} = 5$dB as a typical value for the maximum Gain for an helix isotropic antenna. [39] Then, by reversing the following equation, the length is estimated:

$$G_{LGA} = 10\log\left(\frac{D^2 L}{\lambda^3}\right) + 20.2 \tag{20}$$

The LGA length is $L = 3.98$cm Finally the beamwidth of the antenna can be computed, knowing both the diameter and the length, as:

$$\theta_{LGA} = \frac{16.6}{\sqrt{D^2 L/\lambda^3}} = 95.52^\circ \tag{21}$$

To continue the sizing process of the LGA it was considered a transmitted power of $P_{tx,LGA} = 3.2$W [44] and a new efficiency related to the helix antenna and equal to $\mu_{helix} = 0.7$. [39] Then, following the same equations and assumptions used before for the sizing of the HGA, the subsequent results were obtained:

	Downlink	**Uplink**
E_b/N_0	21.48 dB	37.86 dB
SNR	3.03 dB	22.79 dB

Table 16: LGA results

As shown in the Table 16 the obtained values satisfies both the Error per bit to Noise density and the Signal to Noise Ratio margins.

4.7 Mass budget

According to the general volume characteristics of a common S-band TTMTC subsystem available in literature [77], the mass budget can be evaluated as the 1.5% of the overall mass, which corresponds to 27.95 kg. Moreover, from the available chart regarding the respective Solid State amplier [77], also the mass of the latter is estimated as 1.1 kg which represent a little fraction of the total mass budget related to the TTMTC subsystem.

5 AOCS

5.1 AOCS Architecture

SOHO Attitude and Orbit Control Subsystem (AOCS) provides the spacecraft with the means to point the spacecraft optical reference axis X_o accurately to the sun, control the roll angle and maintain sun pointing within a specified accuracy, perform orbit maneuvers and maintenance, provide an autonomous safe mode and generate measurements via telemetry to ground.

The perturbation torques are due to solar radiation pressure, thrusters misalignment, spacecraft flexibilities, fuel sloshing, tape recorder, experiments, and the High Gain Antenna. The AOCS comprises sensors, actuators, electronics, and software for attitude determination and control.

The AOCS architecture is structured as follows:

- Attitude and orbit sensors
- Attitude and orbit control algorithms
- Attitude and orbit control actuators

5.1.1 Attitude and orbit sensors

The attitude and orbit sensors are the following:

Component	Manufacturer	Number	Redundancy level
HR-STR [1]	Leonardo SpA	2	1
FPSS [14]	Redwire Space	2	1
FSPAAD [3]	*Not specified*	*1*	0
CSPAAD [3]	*Not specified*	*1*	0
Gyroscope [30]	*Not specified*	3	0
Sun acquisition sensor	*Not specified*	0	1

Table 17: Attitude Sensors

The goal of the Fine Pointing Sun Sensor and the High-Resolution Star Tracker is to provide the data for computing the spacecraft attitude, respectively **FPSS** in pitch and yaw axes and **SSU** for the roll axis. The selection of these particular sensors was made with careful consideration of the stringent pointing requirements.

The **HR-STR** is a high-accuracy (better than $1''$), narrow-field star tracker based on an optical system with a catadioptric objective built with radiation-hardened glasses. On the other hand, the FPSS offers 2 measurement axes that enable high-accuracy attitude determination. It provides unambiguous sun angle data immediately upon application of power and it was designed for continuous sun-stare operation.
Given their fundamental role in establishing precise attitude and pointing, both the FPSS and HR-STR are equipped with a redundant counterpart[2].

The AOCS design is based on using independent hardware for anomaly detection: **FSPAAD**, that triggers when the Sun off-pointing is larger than 5°, and **CSPAAD** if it's greater than 25°. Their function is crucial as they enable the determination of when pointing errors reach critical levels for solar panel electricity generation, and consequently, for the survival of the mission.

The spacecraft roll axis is normally pointed toward the Sun, and the three gyros are aligned to measure incremental changes in the roll attitude. **Gyro** calibrations are performed periodically to accurately determine the draft bias associated with each of the three roll-axis gyros, in order to allow the ACU to determine the actual motion of the spacecraft and to maintain the correct orientation. Gyro usage is kept to a minimum because these components are mechanical and subject to wear, and therefore life-limited.
The gyros are not required during most of the mission: they are used only for thruster-based activities such as momentum management, Initial Sun Acquisition (ISA), and Emergency Sun Reacquisition (ESR). In particular:

- Gyro A - Connected to FDE (Fault Detection Electronics) for roll rate measurements for ESR using thrusters. Therefore rigth after calibration is deactivated (despun) in order to conserve its life;

- Gyro B - Connected to FDE for roll anomaly detection
- Gyro C - Connected to Attitude Control Unit (ACU) for roll attitude during computer-based control modes using thrusters

After 1998, when the failure of all the operational gyroscopes occurred, a gyroless mode of operation has been developed (Coarse Roll Pointing 5.3.4).

5.1.2 Attitude and orbit control algorithms

The Normal Mode controller ensures accurate X-axis sun pointing during normal on-station operations. The stringent requirements are on lateral axes, pitch, and roll, which employ the same controller structure. The attitude error is computed by combining the pitch attitude, ensured by the FPSS, and the off-set pitch attitude demands. The resultant error is passed through a second-order phase advance filter and summed with an integrator output, the sum is then multiplied by the gain K to determine the torque demand around the pitch axis. The system exhibits a low overshoot to the specified disturbance and provides ample margins for stability [76].

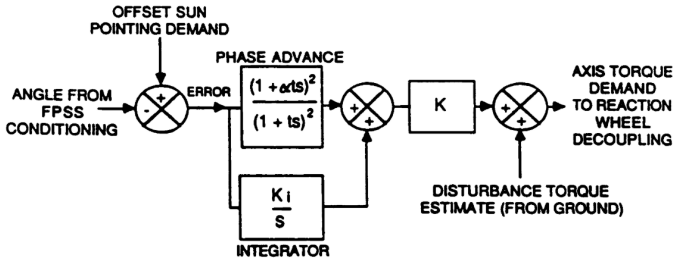

Fig. 9: SOHO normal mode controller

	Pitch	**Roll**
α_t	0.66	0.6
t	0.2	0.125
K	5623	-
K_i	-	3467

Table 18: Controller parameters

5.1.3 Attitude and orbit control actuators

As previously explained, being a 3-axis stabilized spacecraft, the SOHO satellite requires an Attitude and Orbit Control System (AOCS) to ensure also the presence of the following actuators:

Component	**Manufacturer**	**Number**
W45E-RW	Bradford Space	4
MRE-1.0 Monopropellant Thruster	Northrop Grumman Corporation	2 sets of 8

Table 19: Attitude Actuators

Reaction weels W45E Reaction wheels operate as momentum wheels capable of maintaining a constant rotation speed while storing a significant amount of angular momentum for the satellite. As a result of the conservation of angular momentum, once a reaction wheel is spun up, the spacecraft rotates in the opposite direction around the axis of that wheel, restoring the satellite's alignment. Even though the four reaction wheels are arranged in a pyramidal configuration around the x-axis, only three of them are used for attitude control of the SOHO spacecraft, with the fourth serving as a redundancy.

Thrusters Thrusters are utilized in place of momentum exchange devices when disturbance torques surpass the control capabilities of such devices. The reaction control system can activate certain rocket thrusters to control the spacecraft's attitude during thrusting or coasting phases. The goal within the control loop is to either maintain a specific attitude or regulate the rate of attitude change.

ACDS architecture : Based on the actuators choice the architecture for the nominal operations appears to be the **zero momentum** method. This enables unlimited pointing capability in any direction and one of the highest pointing accuracy, limited only by the sensors, that can reach up to 0.0001°. On the other hand this method requires heavy, complex and power hungry hardware to be effective.

5.2 Pointing error budget

A pointing error can be considered as response of a system to external or internal physical phenomena affecting the system pointing performance. As these performance data are scarcely available only the HOP phase has been considered, in particular in the nominal fine pointing mode, which is the most strict in terms of pointing requirements:

Phase	Subsystem	Error index	Error value	Window
HOP	P/Ls	AKE	$X_{pi} : 5'$	/
		RKE	$X_{pi} : 10''$	180 d
		RKE	$X_{pi} : 1''$	15 min
		AKE	$X_a^{roll} : 15'$	/
		RKE	$X_a^{roll} : 1.5'$	15 min
	HGA	AKE	$0.7''$	/ 1

Table 20: Pointing budget error[44] (all values are 3σ)

where $_{pi}$ axes refer to the payload interface reference frame: defined as being nominally parallel to the Sun pointing direction of the experiment sensor and to be in ground alignment with X_B principal axis; and $_a$ to the absolute reference frame (in particular X_a is along the spacecraft-sun line and oriented towards the photometric centre of the Sun).

Building a more accurate pointing error budget would require low-level hardware-specific information not available to at the moment. The cumulative errors presented in Tab. 20 are though an equivalent representation of the pointing performance indexes required by the payload.

5.3 Control modes

The following outlines the respective role of the on-board sensors throughout each SOHO's pointing mode[4]:

5.3.1 Orbital Maneuver Mode (OMM)

The core of the orbital maneuver mode is reached through the initiation of MCC1 and MCC2 orbit correction maneuver and continues with HALO orbit insertion maneuvers. During those delta-V maneuvers, thrusters aligned parallel to the z-axis (mainly Jet7 and Jet8) are used for roll control, while thrusters aligned parallel to the x-axis (Jet1, Jet2, Jet3 and Jet4) are respectively applied for pitch and yaw adjustments. Working together, they continuously help determine the correct attitude control trim maneuvers. Overall, cooperative control strategies integrate reaction wheels and thrusters in orbital maneuvers to efficiently control spacecraft motion. Indeed, thruster firings during orbital maneuvers can be impacted by errors and disturbances, resulting in parasitic torques, leading to the use of reaction wheels for a counterbalanced action.
By combining these two methods, spacecraft can achieve precise maneuvers while conserving propellant for longer missions.
During the transfer phase, ISA is also performed, by means of the Sun acquisition sensors (FSPAAD and CSPAAD). Right after the AOCS subsystem starts to fully operate.

5.3.2 Normal Mode (NM)

The Normal Mode is used to establish and maintain accurate sun pointing during normal operation. In NM, attitude is controlled by adjusting the speed of three reaction wheels arranged in a triangular configuration. The inputs to the control mechanism come from FPSS and the star tracker, oriented 90 degrees away from the Sun direction. The "Roll Steering Law" (RSL) dictates the movement of the stars in the star tracker to keep SOHO oriented exactly in line with the Sun's North-South axis.

5.3.3 Emergency Sun Reacquisition (ESR)

During large parts of the mission, coverage by ground stations is limited. The AOCS has therefore to provide, an autonomous safe mode called Emergency Sun Reacquisition Mode (ESR) in order to protect instruments and the whole spacecraft in case of a hazardous deviation from the nominal attitude conditions resulting from a procedural or hardware failure.

In ESR, the spacecraft attitude is controlled entirely by hardware that senses the approximate position of the Sun and fires thrusters autonomously to ensure that the spacecraft is pointed toward the Sun ($\pm 2^\circ$ on each axis). The reaction wheels are not used autonomously by the spacecraft and they spin down after a certain time. In the process, they impart their angular momentum on the rest of the spacecraft, which is counteracted by the thrusters firings when the pointing reaches the 2-degree limits. After the wheels are spun down, the spacecraft pointing oscillates within the limits.

Through ground intervention, however, the reaction wheels can be spun up (this is part of a normal recovery). They then provide gyroscopic stability to the spacecraft. When tuned correctly, the spacecraft can be left in ESR mode with wheels spun up with practically no thrusters firings. In this mode, the pointing is not strictly controlled, it will drift slowly within the limits, or it can be adjusted by ground control (spinning up/down reaction wheels).

5.3.4 Coarse Roll Pointing (CRP)

The Coarse Roll Pointing is a transitional mode and the first step up from ESR. The spacecraft employs reaction wheels for both attitude determination and roll control, eliminating the need for thruster firings, and pitch and yaw adjustments are determined via the FPSS.
After the failure of the on-board gyroscopes triplet, their functionality has been replaced by a clever software workaround: both roll control and attitude determination rely on the reaction wheels. By leveraging the principle of angular momentum conservation, any deviation in the SOHO's rotation can be detected through changes in the reaction wheel speeds. Remarkably, the roll control achieved in this mode surpasses the accuracy of previous modes utilizing gyroscopes by two orders of magnitude, making SOHO the first three axis-stabilised ESA spacecraft to be operated without a gyro.
In such a mode, SOHO can be instructed to accurately align with the Sun and maintain stability for star mapping via the star tracker, enabling determination of the absolute roll. Subsequently, commands can be issued to readjust the roll orientation back to near-nominal values.

5.3.5 Rotating momentum Wheels (RMW)

In the Rotating Momentum Wheels (RMW) mode, which constitutes an intermediate phase between CRP and Normal Mode, SOHO relies on inputs from both the Fine Pointing Sun Sensor (FPSS) and the star tracker for orientation control. This configuration grants SOHO comprehensive awareness and authority over its positioning. However, compared to CRP, the steering laws are somewhat more lenient, and strict alignment with Solar North-South isn't rigorously enforced. RMW mode is primarily utilized for thruster maneuvers: both Station Keeping (SK) and Momentum Management (MM) maneuvers.

5.4 AOCS subsystem sizing

In order to initialize and perform a correct sizing of the on-board actuators, considering an extended nominal life for SOHO of 6 years and SRP as main acting disturbance, inertia matrix is computed, modeling the spacecraft as a parallelepiped. Panels are considered to be symmetrically deployed with respect to the centre of mass (as in 10)and their thickness is taken into account.

$$I = \begin{bmatrix} 3758 & 0 & 0 \\ 0 & 4916 & 0 \\ 0 & 0 & 4423 \end{bmatrix} \text{kg m}^2$$

	L_x	L_y	L_z	Mass
Main body	4.3 m	2.7 m	3.7 m	1811 kg
Solar panels	7 mm	3.4 m	3.7 m	51.83 kg

Table 21: Controller parameters

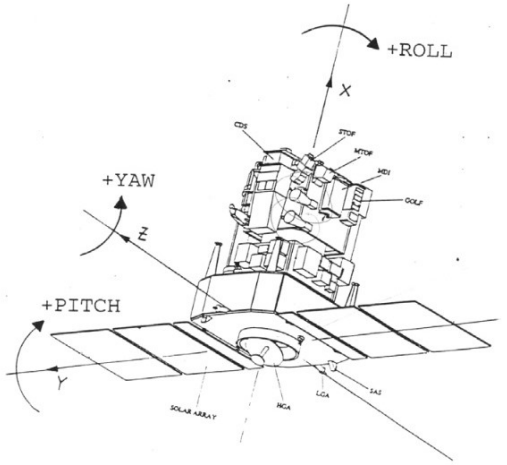

Fig. 10: SOHO normal mode controller

The overall inertia matrix is as shown, with the maximum inertia axis coincident with the y-axis.

5.4.1 External disturbances torque

Given SOHO's orbit characteristics, the main external disturbance to be controlled by the on-board reaction wheels is the torque generated by the solar radiation pressure.
A simple model has been computed to have an estimation of the SRP's effect:

$$T_{SRP} = \frac{F_s}{c} \cdot \left(A_{s/c}(1+q_{s/c})(x_{CM,s/c} - x_{CP,s/c}) + 2A_{pan}(1+q_{pan})(x_{CM,pan} - x_{CP,pan}) \right) = 2.0335 \cdot 10^5 \text{N m}$$

Where the reflectance factor q is respectively 0.5 and 0.3 for spacecraft external surfaces and solar panels, while $F_s = 1411\,\text{W m}^{-2}$ is the solar constant at L1 distance, and $(x_{CM,s/c} - x_{CP,s/c}) = 0.07\,\text{m}$ is the offset between the centre of solar pressure and the centre of mass of the spacecraft, which is assumed to be coincident with the origin of reference axis, while for the solar panels $(x_{CM,pan} - x_{CP,pan}) = 0.1\,\text{m}$ [59] [10]. In order to withstand the effect of the resulting torque, each one of the 3 nominal reaction wheels will store along an L1 orbit period of about 178 *days* [17] an angular momentum $h_{RW,stored} = 208.49\,\text{N m s}$ by taken into account a safe margin of 100% on the SRP disturbance.

From [24] the maximum angular momentum of the Reaction Wheels is taken as 40 N m s. Therefore desaturation has to be performed around every 0.19 orbits, e.g. approximately every 34.1 days (overestimated). The obtained value consists in an approximation since the actual values of the offsets were not available and furthermore it was considered the maximum value of the SRP torque acting throughout the entire period.

5.4.2 RW desaturation

By considering a nominal value of nominal thrust T = 4.4 N[20] for each thruster, the needed de-saturation time and then the propellant mass are obtained:

$$t_{des} = \frac{h_{RW,max}}{2bT} = 2.11\,\text{s} \qquad m_{p,des} = \frac{t_{des}T}{I_{sp}g_0} = 0.004\,\text{kg} \tag{22}$$

Furthermore a 20% safe margin to better estimate the number of orbits after which the saturation is needed was considered. Regarding to the six years of nominal life the estimated used propellant mass to de-saturate the three reaction wheels is 0.505 kg.

5.4.3 Internal disturbances torque

The on-board perturbations that the control also has to counteract are mainly due to: change in mass distribution, related to the gradual emptying of propellant tanks and sloshing; payload and actuators misalignment and position uncertainties; structural dynamics due to flexibility of the extended panels.

Among all the internal disturbances effects, one of the most demanding is the thrusters misalignment which produces great instability effects on the spacecraft. To estimate the amount of torque it was taken the worst estimated value: $\theta_{mis} = 0.5°$.[39] Since during the de-saturation mode the thrusters were used continously, it was decided to consider the firing time equal to the de-saturation time, therefore the torque can be estimated by inverting the Equation 23: $T_{t,mis} = 38.4\text{N m}$, then each reaction wheels stores $h_{RW,mis} = 27.05\text{N m s}$.

As done in the section 5.4.2, the estimated propellant mass for the nominal life is found: $m_{p,mis} = 0.135\,\text{kg}$

5.4.4 Slew maneuver

After the insertion in the operational orbit, the spacecraft might need a slew maneuver prior to the activation of the 3-axis stabilizing control.
To compute the propellant mass used for the slew maneuver, the worst condition is taken into account: the Maximum Torque is taken from RW datasheet[24] while the rotation angle is considered as the maximum possible around the yaw axis (180 deg). To evaluate the minimum time to perform the maneuver it was decided to approximate the computation by taking into account the maximum Inertia moment:

$$t_{slew,min} = \sqrt{\frac{4\theta_{max} I_{max}}{T_{rw,max}}} = 499.1\,\text{s} \tag{23}$$

from which the angular rate $\dot{\theta}_{max} = 0.36\ ^\circ\,\text{s}^{-1}$.

Since slew maneuvers is performed with maximum two thrusters per time and by imposing the rotation around the yaw axis, the propellant mass utilized for each maneuver is estimated with the Equation 24 to obtain $m_{p,slew} = 0.004\,\text{kg}$.

5.4.5 Station keeping maneuver

Regarding the station-keeping maneuvers performed by SOHO, the propellant mass was estimated from the Tsiolkovsky equation by considering the six years nominal life with a total $\Delta V = 34.02\,\text{m s}^{-1}$ and it was obtained: 29.14kg.

5.4.6 Sensors and Actuators position

The position of the sensors and actuators has been established by means of a literature review and AOCS subsystem sizing.
Sensors

- **HR-STR**: is oriented 90° away from the Sun to avoid, as much as possible, any noise from sunlight; [3]
- **FPSS**: pointing towards Sun direction (+ X_0 axis);[3]
- **FSPAAD** and **CSPAAD**: directed as the aforementioned FPSS towards the Sun direction to exploit their sun acquisition function;
- **Gyros**: Oriented as the principal inertia axis of the spacecraft;

Actuators

- **RW**: triangle configuration with a redundant wheel(RW 3). This configuration was chosen to compensate better the effect around pitch axis, where the biggest component of SRP torque is expected. The configuration guarantees stabilization also around roll and yaw axes but with a less needed compensation;
- **Thrusters**: orientation of thrusters was already outlined in Propulsion subsystem;

5.5 Subsystem budgets

5.5.1 Mass budget

To compute the AOCS subsystem mass budget Gyros masses were assumed by considering similar applications in terms of total mass, satellite type and SOHO contemporary applications. The FSPAAD and the CSPAAD masses were considered negligible as they act only as triggers. The other components masses were taken from datasheets.

Component	**Mass** kg	**% Total mass**
Sensors		
2 HR-STR [1]	14.4	0.77%
2 FPSS [14]	1.9	0.13%
FSPAAD [3]	-	-
CSPAAD [3]	-	-
3 Gyroscopes [30]	6	0.32%
Actuators		
3 RW	26.8	1.44%
16 Thrusters	8	0.43%

Table 22: Mass budget

The total mass budget for the subsystem is then 57.1 kg, which constitutes 3% of the overall spacecraft mass.

5.5.2 Power budget

An estimation of the power budget required for the AOCS subsystem is provided by taking into account the most demanding scenario: e.g. reaction wheels working at their maximum speed [24]and 4 thrusters firing to ensure full attitude control. The total power budget for the AOCS subsystem can be calculated referring to the most demanding operation, which is desaturation, when all the sensors are active and a couple of thrusters is firing, while the three reaction wheels are still in function. Therefore the resulting power demand of 157.95 W, 10.5% of the mission power budget, which is consistent with the percentage of power budget reported in literature for analogous missions [39].

Component	**Power** [W]	**% Tot PB**
Sensors		
1 HR-STR [1]	5	0.33%
1 FPSS [14]	0.25	0.02%
FSPAAD [3]	-	-
CSPAAD [3]	-	-
3 Gyroscopes [30]	30	2%
Actuators		
3 RW	87	5.8%
8 Thrusters	71.4	4.76%

Table 23: Power budget

5.5.3 Data budget

The analysis on data volume regards the capacity of the sensor to store data in terms of byte. For the star tracker and the gyroscopes reliable values were assumed in the absence of the references ones.

Components	HR-STR	FPSS	3 Gyroscopes
Data Volume[B]	8	8	4.5

Table 24: Data budgets

The total estimated data volume is 20.5 B.

6 TCS

6.1 TCS architecture

The SOHO spacecraft consists of two independent subassemblies, the payload module (PLM) and the service module (SVM), with their own thermal control subsystem, respectively PTCS and STCS.
The Thermal Control Subsystem (TCS) is required to:

- Keep the temperatures of the spacecraft subsystems and instruments within specified temperature limits during all expected mission phases and operation modes;
- Provides stable thermal environment in order to meet all the pointing requirements of the AOCS and experiment sensors;

The adopted Thermal Design philosophy is based on the use of classical passive techniques (MLI, painting and radiators), different for each module and equipment in order to maintain their specific operational temperature intervals 26 (mainly available in SOHO mission literature or assumed within typical ranges), which in general stay in a common range except for CDS detector with its very low temperature requirement and the propulsion system.

Radiators are widely exploited as passive control technique, since deep space ensures continuous heat sink throughout the entire mission. Heat sources slightly change along the phases: Earth albedo and IR fluxes become almost negligible right after the insertion in the transfer orbit and until the rest of the operational phase in halo orbit. Solar direct flux can be considered almost constant according with solar panels pointing requirements and non-presence of eclipse transients.

Phase	**Heat Source**	**Heat Sink**
TTP	Sun, Internal Power, Earth albedo, Earth IR	Deep Space
HOP	Sun, Internal Power	Deep Space

Table 25: External and internal thermal fluxes with phases

6.2 Payload module

To meet the above requirements, a mix of multi-layer insulation (MLI), coatings and heater circuits have been defined: the PLM external surfaces are covered with MLI consisting of 13 layers. The outer layer is made of carbon filled Kapton and the inner layers are made of Mylar or Kapton. The PLM internal surfaces are also black painted in order to allow good predictable radiative coupling and to minimize temperature gradients.

The basic concept of the PLM thermal control is to use a heater fixed power mode with adjustable power levels for each heater circuit which is controllable from the ground. Indeed, all experiment sensor units (except VIRGO) perform their own thermal control, i.e. they're isolated from the S/C structure through isostatic mounts. The PLM thermal control thus only guarantees the temperature range of their temperature reference points. To this aim, the instrument sensors are mounted in the 4 upper lateral panels: $\pm Z$, $\pm Y$ panels and the $+X$ panel under the sunshield. Those panels are covered with MLI blankets. For the other units, i.e. VIRGO and all electronic units (except MDI and LASCO electronics), the PLM is in charge of the full thermal control.

Component	**T range** [°C]
Optical payloads [44]	20 ± 1
General instruments [19]	$-15 \div +30$
CDS detector [44]	$<$ -70

Table 26: Payload temperature ranges

6.3 Service module

SOHO's service module houses all the vital systems needed for the optimal operations of the payloads. As per [60] three main sections have been identified:

- Lateral panels and lower platform: radiators are located on these panels. What is not covered by radiators is covered with MLI that is coated with white PSG120FD paint [23]that was selected because of the high emissivity/absortivity ratio. The $\pm Y$ panels also receive reflection from the Solar Arrays;

- Upper platform: solar inputs will be minimized by using thermal blankets on upper platform. The external sheet of this MLI is coated with black Electrodag 501C paint[12] to reduce as much as possible the solar reflection-to the PLM;
- Internal structure: internal SVM temperature homogeneity is achieved using a black paint coating.

In general doublers, interfillers and thermal strap have been used locally to increase the heat flow from specific units to radiator panels.
This basic design is complemented with heater lines, controlled by thermistors, to heat units such as the Hydrazine tank, RCS pipes and PLM-SVM interface ring.

Component	**T range [°C]**
LGAs [25]	$-40 \div +80$
HGA [39]	$-100 \div +80$
Solar Panels [39]	$-100 \div +150$
20 Ah NiCd batteries [39]	$-10 \div +25$
Electronics [13]	$-20 \div +40$
Tanks and feeding lines[39]	$+15 \div +40$
Reaction Wheels [39]	$-10 \div +40$
Gyros and Star trackers [39]	$0 \div +30$

Table 27: Service module temperature ranges

6.4 TCS subsystem sizing

The analysis starts from the SOHO separation in TTP since from Launch to the LEOP the spacecraft is still connected with the CENTAUR launcher. Earth albedo and IR effect becomes minor along the TTP, while internal power reaches a maximum during the Halo Phase, when all the payloads are operative.

6.4.1 Thermal environment

A preliminary analysis on the thermal environment encountered throughout the mission has to be performed in order to distinguish and define both the hot and cold cases. First of all the major thermal sources are identified:

$$q_{sun} = q_0 \left(\frac{R_{Earth}}{R_{Sc}}\right)^2 \qquad q_{albedo} = q_{sun} \cdot a \cdot cos(\theta) \left(\frac{R_{pl}}{R_{orbit}}\right)^2 \qquad q_{IR} = \sigma \cdot e \cdot T_{pl}^4 \left(\frac{R_{pl}}{R_{orbit}}\right)^2 \tag{24}$$

Where an average albedo factor $a = 0.35$ is assumed, and $e = 0.8$ is the computed value for the infrared emittance. The next step is to evaluate heat powers, assuming the spacecraft as a rectangle parallelepiped, where cross and radiating sections were computed from the size of the spacecraft. [44]

$$Q_{sun} = q_{sun} \cdot A_{cross} \cdot \alpha \qquad Q_{albedo} = q_{albedo} \cdot A_{cross} \cdot \alpha \qquad Q_{IR} = q_{IR} \cdot A_{cross} \cdot \epsilon \tag{25}$$

6.4.2 Cold case

The cold case has been located along the transfer orbit, after around 10 days after the separation from the upper stage, when on-board instruments aren't yet completely operative and so the generated internal heat is at minimum. Moreover the distance from Earth is enough for the albedo and IR thermal flux contributions to be considered negligible.

6.4.3 Hot case

The hot case is the operational one, reached in the halo orbit phase. All payloads are switched on and fully operative and also maximum values of Sun heat power are experienced.

6.4.4 Mono node analysis

A first preliminary thermal analysis has been carried out adopting a mono node approach, where both the modules aren't considered independently but as a whole. The radiating area $A_{radiating}$ is considered to be the whole external surface, except for the $+X$ face where the sun-shield is placed.
For the sake of simplicity $A_{cross} = 9.99\text{m}^2$ is assumed to be the $+X$ surface, as if it was always perpendicular to the Sun. For the hot case configuration this is almost exactly while in the cold case this could be considered partially inaccurate, however this appears reasonable given the fact that possible de-pointing of the assumed configuration would result in a less effective protection of the shield, so in an increasing of the spacecraft temperature with consequent overestimation of the cold case.

6.4.5 Coating

The MLI coating was designed according to literature information found in [44]. The outer layer is made of Carbon Filled Kapton, the eleven internal layers are made of both Aluminized Mylar (six layers) and Aluminized Kapton (five layers) while the inner layer is made of Kapton for a total number of thirteen layers out of reciprocal contact to ensure radiation only. From the emittance and the absorptance of the single layers the equivalent values are computed as:

$$\epsilon^* = \frac{1}{1/\epsilon_1 + 1/\epsilon_2 - 1}\left(\frac{1}{N+1}\right) \qquad \alpha^* = \frac{1}{1/\alpha_1 + 1/\alpha_2 - 1}\left(\frac{1}{N+1}\right) \tag{26}$$

Since the spacecraft is moreover protected by a sunshield to reduce the heat amount absorbed by Sun radiation, this further element was taken into account. To reduce as much as possible the absorbed radiation by the sunshield a very small absorbivity coefficient was considered, selecting a compatible material: ITO-CMX Ag-NiCr. [22]

	CFK	**Al Mylar**	**Al Kapton**	**Kapton**	**Sunshield**
$\boldsymbol{\alpha}$	0.95	0.175	0.105	0.38	0.085
$\boldsymbol{\varepsilon}$	0.84	0.05	0.03	0.67	0.83

Table 28: Emittance and absorptance coefficients[39][5][41][10]

The emittance values for Aluminized Mylar and Aluminized Kapton are taken for the total number of internal layers since no further specification about upper and inner surfaces were available. By computing the effective emittance and absorptance with Equation 26 the obtained values are: $\epsilon = 0.0189$ and $\alpha = 0.0375$.

6.4.6 Radiators and Heater Sizing

Hot case: the temperature that would be achieved in the halo orbit is:

$$T_{Hot} = \left(\frac{Q_{sun} + Q_{int,max}}{\sigma \cdot A_{radiating} \cdot \epsilon} + T_{DS}^4\right)^{\frac{1}{4}} + T_{margin} = 403.8\,\mathrm{K} \tag{27}$$

Where $T_{margin} = 5\,\mathrm{K}$ is the safe acceptance margin taken into account. [39]
$Q_{int,max} = 1236\,\mathrm{W}$ includes the internally generated power for PLM TCS, instruments, SVM TCS, SVM S/S, and losses [36]. But taking into account the temperature limits achievable by the on board equipment, a reasonable temperature value reachable by the spacecraft is assumed to be $T_{max} = T_{SC} = 20\,^\circ\mathrm{C}$. Therefore it's necessary to size radiators to dissipate the extra heat contained in the spacecraft. In order to evaluate the overall A_{rad} the following formula is then used:

$$A_{rad} = \frac{Q_{int,max} + Q_{sun} - \sigma\epsilon_{SC}A_{SC}(T_{max}^4 - T_{DS}^4)}{\sigma(\epsilon_{rad} - \epsilon_{SC})\left(T_{max}^4 - T_{DS}^4\right)} = 3.46\,\mathrm{m}^2 \tag{28}$$

where $A_{SC} = A_{radiating} = 65.03\,\mathrm{m}^2$, $T_{DS} = 3\,\mathrm{K}$ is the deep space temperature.
$\epsilon_{rad} = 0.88$ as the solid surface of the radiator is made out of Black painted Kapton that guarantees very high performances in terms of emittance. The selected values was taken from datasheets on black paints usually used on Kapton layers[41]. Finally the computed total area of radiators is coherent with respect to spacecraft available surface.

Cold case: the necessity of active thermal heaters has to be evaluated in the cold case scenario, taking into account the presence of radiators. Furthermore a $T_{margin} = -5\,\mathrm{K}$ safe acceptance margin was considered. [39]

$$T_{Cold} = \left(\frac{Q_{sun} + Q_{int,min}}{\sigma \cdot (A_{sc}\epsilon_{sc} + A_{rad}\epsilon_{rad})} + T_{DS}^4\right)^{\frac{1}{4}} + T_{margin} = 265.2\,\mathrm{K} \tag{29}$$

where $Q_{int,min} = 757\,\mathrm{W}$ is obtained by subtracting the instruments contribution from the total internal power [36]. According with the allowable highest minimum temperature among the components: $T_{min} = T_{SC} = 15\,^\circ\mathrm{C}$. From the previous sizing, $A_e = A_{SC} - A_{rad} =$ is easily computed and used for the heaters sizing as it follows:

$$Q_{heaters} = \sigma \cdot (\epsilon_{sc}A_e + \epsilon_{rad}A_{rad}) \cdot T_{min}^4 - Q_{IR} - Q_{int} = 372.88\mathrm{W} \tag{30}$$

which is consistent from what is expected from literature.[36]

6.5 Mass budget

Starting from the mono-nodal sizing results, a preliminary mass budget is performed.

Component	**Area**[m^2]	**t** [mm]	ρ[g/cm^3]	**Mass**[kg]	**Margin**[39]	**Mass with margin**[kg]
Sun-shield [16] [22]	9.99	0.5	7.14	35.66	10 %	39.23
Radiators [11]	3.46	0.125	1.42	0.61	50%	0.92
MLI [21]	57.61	0.078	1.4	6.29	5 %	6.61
TCS mass with margins[kg]				46.76		

Table 29: Mass Budget

The sun-shield area is assumed to be equal to the surface in the $+X$ direction and the MLI area is the radiating surface excluding the radiators and the sun-shield area, this assumption overestimates the real mass of the TCS. The thicknesses and the densities are chosen from data sheets of current applications, in particular, the MLI density used is a mean between the Kapton and the Mylar density. Due to their lighter weight, the heaters are neglected. In the end, a 5 % design maturity mass margin is applied to MLI because it has already been used in several space applications, a 10 % margin for the sun-shield because of the specific arrangements that have to be taken into account for the constant sun pointing crucial to the mission success, and 50 % for the radiators because their area has been obtained as result of the coarse phase A analysis. The TCS percentage of the total mass (1863 kg) equal to 2.51% is consistent with analogous applications [39].

6.6 Power budget

Component	**Power**[W]	**% Tot PB**
PTCS	170	11.33 %
STCS	133	8.8 %

Table 30: Power budget

The total power budget reserved for the Thermal control system is the 20.13 % of the total. This value could be considered partially consistent with the percentage of power budget reported in literature for analogous missions.[39]

6.7 Data budget

Temperature sensors (thermistors) are, among the others, required to keep track of spacecraft's status and they're data are collected periodically along a 3.7 h time window with an estimated housekeeping rate of 0.13 kbit s^{-1} (10% of the total housekeeping rate, which includes also attitude sensors). An additional 50% margin is added to overestimate the required memory capacity required on board for the housekeeping data volume [39], that results to be 0.32 MB per operational day.

6.8 Multi-node Thermal Analysis

In order to enhance our understanding of the mission's thermal control system, a more comprehensive analysis is undertaken. This analysis involves a multi-node thermal division of the PLM, with a focus on two potentially significant aspects:

- Parts of the system with specific operational temperature requirements.
- Components of the system characterized by significant thermal power generation.

To facilitate this analysis, the actual dimensions of each node of the system were obtained from NASA's Soho 3D model [37]. A scale factor was applied to these measurements to calculate the real dimensions. The analysis begins by dividing the system into two subsystems: one for the PLM and one for the SVM. This division disregards the heat exchanged by these two systems, justified by:

- The interface ring between PLM and SVM is mantained at $20 \pm 5°C$ and PLM is thermally decoupled from the SVM propulsion ring through insulation washer[36].
- Solar reflection from the SVM to the PLM is minimized by utilizing the SVM upper panel's external sheet of MLI, which is black painted with Electrodag 501C, ensuring low specularity [60].

6.8.1 Multi-node PLM Thermal Analysis

The PLM system is subdivided into thermal nodes, focusing on parts with specific thermal requirements or significant power generation. The following scheme illustrates this subdivision:

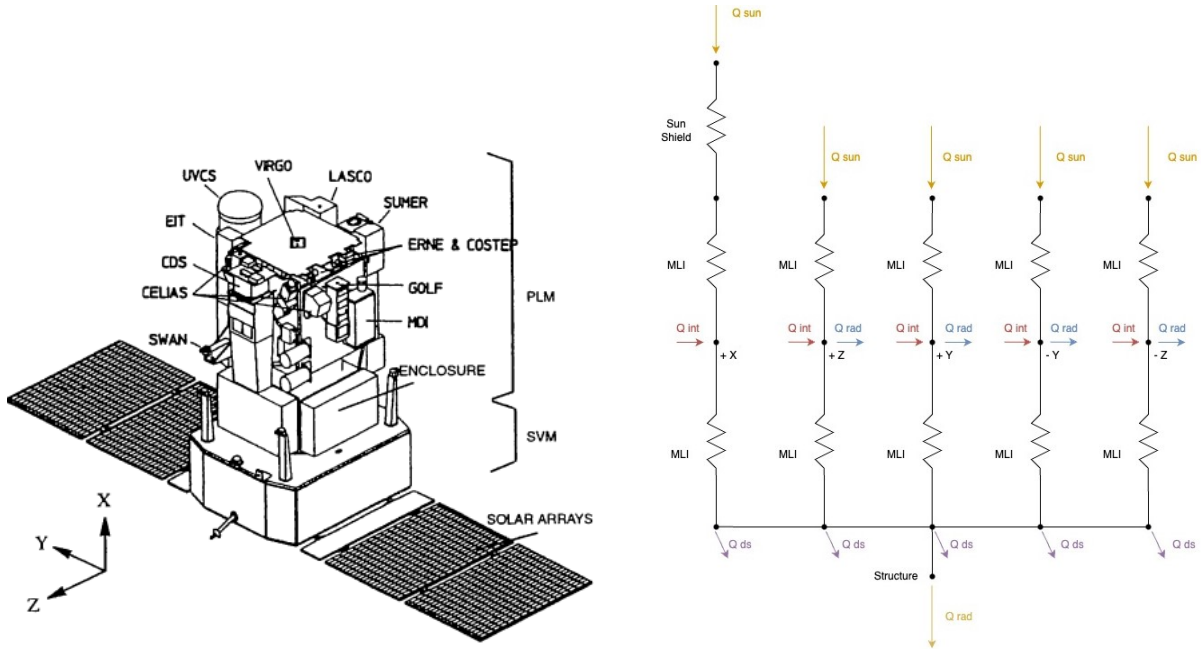

(a) SOHO architecture (b) PLM Thermal resistance scheme

Fig. 11: From SOHO architecture to PLM thermal scheme

The analysis primarily targets payload panels, as they are covered with MLI and generate power due to electronic operations. These payload instruments are divided into panels with specific requirements [44]:

Payload panels	**Instruments**	**Cold case**(°C)	**Hot case**(°C)	**Internal Power**(W)
Panel X	VIRGO	15	30	9.3
Panel +Y	UVCS - EIT	5	30	90.7
Panel -Y	GOLF/MDI/ERNE/COSTEP	10	35	174.0
Panel +Z	CDS/CELIAS/SWAN	10	30	114.3
Panel -Z	SUMER/LASCO	15	27	90.7

Table 31: Payload Panels and requirements

For the internal generated power, where instruments data were unavailable, the total remaining power is divided equally for each instrument, considering similar electronics (PLM instruments total power is 479W[36]). The cold case temperature for Panel X considers also the presence of electronics in addition to VIRGO, which alone can withstand lower temperatures (3°C)[44]. Starting from the previously described hot case and imposing requirements on each operational temperature, the aim is to determine the radiators for each payload. Results are obtained by applying Kirchhoff's law at each node, ensuring that the sum of heat exchanged at each node equals zero:

$$Q_{\text{sun}} + Q_{\text{internal}} - Q_{\text{ds}} - Q_{\text{radStructure}} - Q_{\text{radiators}} = 0 \tag{31}$$

The previous heats are defined as before, with the addition of $Q_{\text{radStructure}}$, defining T_p as each panel temperature and $A_{\text{radStructure}}$ the evaluated area of heat exchange with the structure:

$$Q_{\text{radStructure}} = \sigma \varepsilon_{\text{MLI}} A_{\text{radStructure}} (T_p^4 - T_{\text{structure}}^4) \tag{32}$$

Since the PLM structure has a large emission area and limited heat exchange with the payload, its radiator dimensioning is not the focus of this analysis, although it could be included in subsequent analyses. Next, focusing on the cold case, the required heater power for each panel was determined using the following equations at each node:

Payload panels	**Radiator area** (m^2)	**Heaters power** (W)
X	0	19.2
+Y	0.349	16.9
-Y	0.426	67.0
+Z	0.455	65.7
-Z	0.283	68.1
Total	1.513	236.9

Table 32: Radiator Areas and Heaters Power for Payload Panels

A notable consideration is made for the X panel, which is most affected by solar heat. Since it is inside the structure, it cannot directly expel heat through a radiator towards deep space. Therefore the analysis suggests that enclosing it entirely in thick MLI could lead to overheating. To address this, the MLI layers were reduced on the sides (from 13 to 5) and ensure good emissivity in the lower X panel, enabling respectively greater emission towards both deep space and the structure below the panel. The total radiator area computed is 1.512 m^2, consistent with the mono-node analysis, considering the PLM's relative dimensions to the overall structure and the significant solar heat incoming on the subsystem. To conclude the total computed heaters power is 236.9 W, similar to that provided by SOHO specifications for PTCS, 170W [36].

6.8.2 SVM Thermal Analysis

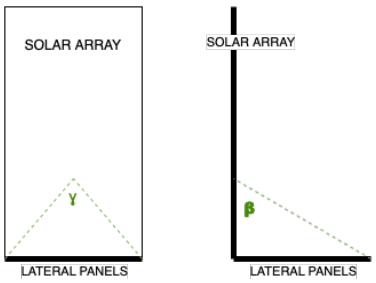

The SVM thermal analysis can be efficiently conducted as a mono-node system due to the following reasons:

- Less Stringent Thermal Requirements: only the Hydrazine tanks require slightly different temperatures, reducing the need for complex multi-node analysis.
- Dominance of Isolated Components: Components such as the RWs, HGA and tanks, which are significant in terms of power generation or thermal radiation, are effectively isolated using specific MLI.

Once again, the equation regulating the thermal performance is:

$$Q_{solar} + Q_{arrays} + Q_{int} + Q_{TCS} - Q^{MLI}_{emitted} - Q^{rad}_{emitted} = 0 \tag{33}$$

where Q_{arrays} represents the heat reflected from the solar arrays onto the SVM lateral panels.
The evaluation of the aforementioned heat flux requires the knowledge of the view factor from the solar arrays to the lateral panels, in other words the percentage of the solar array celestial hemisphere occupied by the SVM lateral panels. By computing the angles shown in the figure, for each value of the longitudinal coordinate of the solar panels this percentage is found to be $\approx 4.95\%$. This value, compounded with a value of reflectance of 5% (taken as an average for solar arrays, as more specific data is not available) is enough to estimate the heat flux reflected by the solar panels. All heat fluxes are pass through a MLI, these have been modeled according to Sec. 6.4.5 using 15 internal layers of Al Kapton 28 and an external coating of the previously mentioned paints whose data is presented in Tab. 33.

	Electrodag 501C[12]	**PSG120FD[23]**
$\boldsymbol{\alpha}$	0.965	0.82
$\boldsymbol{\varepsilon}$	0.19	0.88

Table 33: Paints coefficients

Finally, the spacecraft temperature for the hot and cold case must be determined. These values depends on the SVM units requirements and, unlike with the PLM, do not change drastically between the cold and hot case. This is due to the fact that most units are in a powered state in both states; the only unit that is considered to be off during the cold case is the HGA as it is deployed only in the adavanced state of the TTP phase[66]. Based on Tab. 27 the S/C hot and cold temperature are chosen to be $T_{cold} = T_{hot} = 20\,°C$. The results of Eq. 33 are then presented in Tab. 34 for the cold and hot case:

	$\boldsymbol{Q_{solar}}$	$\boldsymbol{Q_{arrays}}$	$\boldsymbol{Q_{int}}$ [36]	$\boldsymbol{Q_{TCS}}$	$\boldsymbol{Q^{MLI}_{emitted}}$	$\boldsymbol{Q^{rad}_{emitted}}$	$\boldsymbol{T_{S/C}}$	$\boldsymbol{A_{rad}}$
HOT	159.7 W	20 W	424 W	0 W	276.7 W	327 W	20 °C	0.887 m^2
COLD	156.8 W	19.7 W	374 W	53.2 W	276.7 W	327 W	20 °C	0.887 m^2

Table 34: SVM results

7 EPS

7.1 EPS Architecture

The power subsystem provides regulation, protection and distribution of maximum 1400 W of solar-array power [44], supported by two 20 Ah Ni-Cd batteries of 32 cells which are sized to deliver power during initial acquisition phase and for peak power (950 W h).
The primary power source of the mission is the solar array which consists of 2 deployable wings (+Y/-Y), each composed of 2 solar panels and 1 yoke panel, made of Back Surface Reflection (BSR) silicon cell with a resistivity of $2\,\Omega\,\mathrm{cm}$.

SOHO features a fully-regulated three-domain direct energy transfer (DET) control, where any solar array power in excess of load demand is autonomously prioritised for spacecraft battery charging, without the need for intervention by any other spacecraft system[56]. This design is based on three separated domain, namely the S3R, BCR and BDR.

7.1.1 Power Control Unit (PCU)

The main DC power bus of SOHO is regulated to $28\,\mathrm{V} \pm 1\%$ by the Power Control Unit (PCU), configured as an integrated shunt, charger and discharger, direct energy transfer system.

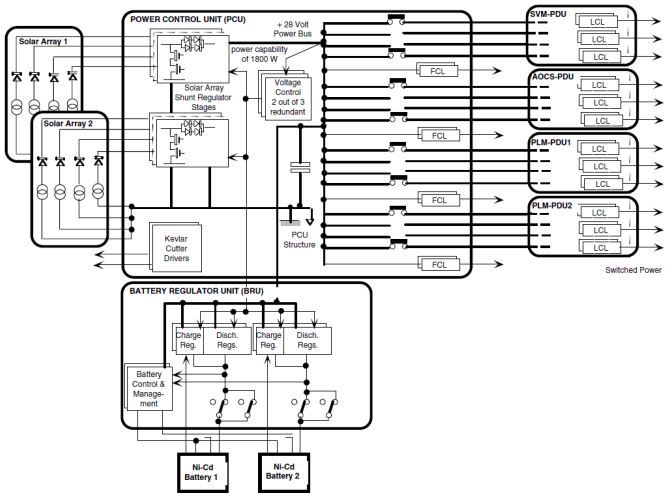

Fig. 12: SOHO spacecraft EPS scheme

The solar array shunt is of the Sequential Switching Shunt regulator (S3R) concept where eight serial redundant dump switches are connected to the corresponding eight electrical sections of the solar array. It selects the number of solar array sections to both supply the total spacecraft load and enable the batteries to be charged in the desired manner.

Also housed within the SOHO PCU is the main bus load switching and power distribution function, this comprised of redundant Foldback Current Limiters (FCLs) for the spacecraft command receivers/decoders and the attitude control failure detection electronics. Additionally conventional power relays are used to effect power bus activation for the four down-stream, Power Distribution Units (PDUs).

7.1.2 Battery Regulator Unit (BRU)

The Battery Regulator Unit (BRU) is a separate equipment which consists of four battery discharge regulators, which act as input current limiters, and two battery charge regulators.
Finally the Battery Regulator Unit also contains the battery management electronics for the two nickel-cadmium batteries.

7.1.3 Power Distribution Units (PDUs)

The four Power Distribution Units (PDUs) provide main bus power to: the service module electronics (SVM), the attitude and orbit control system (AOCS) and two supplies for experiments and heaters on the payload module (PLM1 and PLM2).
Each of these units receives four independent power feeds from the PCU, two of these lines having 12 (redundant) Latching Current Limiters (LCLs) for electronic load/experiment switching and the other two lines having 16 (redundant) LCLs for activating spacecraft heater loads. [45] [56].

7.1.4 Power Demand

The power budget per phase/mode and subsystem is reported here. Furthermore, a 20% system-level margin is added to the nominal power requirements of the spacecraft.[39].

Subsystem	**TTP**	**HOP**		
		Maneuvers	**Communication**	**SO**
PS[40]	53.6	35.7	35.7	35.7
TMTC [40]	0	0	50	0
AOCS [40]	87	122.25	122.25	122.25
TCS [36]	303	303	250	303
Payload [45]	0	479	479	479
Others[39]	125.1	130	129.2	130
TOT	568.7	1070	1066	1070
Margin	+ 20 %			
TOT Margined	682.4	1284	1279.2	1284

Table 35: Subsystems power demand in Normal Mode

Propulsion: four activated thrusters were considered for station keeping maneuvers during scientific observation mode and communication mode and six thrusters as the most demanding case for the transfer maneuvers (MCC2 maneuver);
TTMTC: only communication mode, where the HGA is utilized, is taken into account, while the demanded power of the LGA was considered negligible;
AOCS: in scientific and communication modes only RW, sensors, and gyroscopes are considered; in transfer maneuver phase only the reaction wheels are taken into account;
TCS: during communication mode SVM heaters were turned off as non-needed while in the others considering the not-functioning HGA, the SVM heaters are taken into account with a power of 53 W as dimensioned before;
Payload: the payloads are switched on during all modes of the HOP;
Others: the others subsystems considered are EPS, OBDH and moving mechanisms.

To compute the budgets a certain percentage of the total power budget was taken into account. This value is chosen to be 22% (considering the SOHO spacecraft as belonging to the 'Other' category among the possible kinds of satellites) of the total power budget without considering the payload.[39]

A different analysis should be done for the ESR mode in which some of the considered budgets are different due to the peculiarity of this mode. In the table below all the modified power budgets per subsystem are resumed.

PS[40]	**TMTC**[40]	**AOCS**[40]	**TCS**[36]	**P/L**[31]	**Others**[39]	**TOT**	**TOT Margined**
71.4 W	0 W	87 W	303W	389W	81.4 W	931.8W	1118.2 W

Table 36: Subsystems power demand in ESR Mode

where CDS and SUMER payloads have been considered switched off for the computation of the power budget. [31]

7.1.5 Operational profiles and available sources

The operational profile of the SOHO mission revolves around continuous observation of the Sun, utilizing advanced instrumentation and international collaboration to advance understanding of solar physics and space weather. To achieve it the operational profile of the mission relies on a Halo observation orbit around L1 maintained throughout the whole lifetime. This allows the continuous use of the solar panels as the primary power source.

Secondary batteries are the typical energy storage for spacecraft, which ensure that the power demand is provided even during eclipse periods. According to SOHO mission baselines, solar panels are thought to face the Sun for their entire operational life in Halo orbit; therefore batteries were designed for emergency modes, in case of a significant Sun de-pointing. This approach also allows peak power demands to be furnished

throughout the mission.
Considering the mission's objective, the satellite, in normal mode, is always pointing at the sun. Because of that, the solar aspect angle is assumed to be zero.

Sun Distance [km]	**Irradiation** [W/m^2]	**Solar Aspect Angle** [°]
148097870.7	1395.3	0

Table 37: Available source data during operational phase

7.2 EPS subsystem sizing

7.2.1 Solar array sizing

Since during all phases the satellite is Sun-pointing, no eclipse mode is expected. Therefore, the power to be produced by the solar array is computed only considering the mode requiring the maximum power (P_d for maneuvers and SO) and the efficiency of the power distribution strategy (DET 7.1), for which $X_d = 0.85$ [39]):

$$P_{SA} = \frac{P_d}{X_d} = 1510.6\,\mathrm{W} \tag{34}$$

To obtain the total area of the solar array, the following steps must be followed, in order to account for the successive drop in power generated due to the efficiency of the arrays ($\epsilon_{bol} = 0.132$) [35], their aging (dpy = 0.04) [70], and the mean nominal inherent loss factor ($I_d = 0.77$) [39]).
The initial and the begin of life power are:

$$P_{in} = \epsilon_{BOL} P_0 \quad = 184.2\mathrm{W\,m^{-2}} \qquad\qquad P_{BOL} = P_{in} I_d \cos(\theta) = 141.3\mathrm{W\,m^{-2}} \tag{35}$$

where P_0 is the solar irradiance computed as $P_0 = q_0 \left(\frac{R_E}{R_{sc}}\right)^2 = 1395.3\mathrm{W\,m^{-2}}$. While the solar array angle (θ) is considered as 5°, implementing a very conservative design, even considering the worst condition. Indeed, during all phases the satellite is Sun-pointing, and the worst pointing mode (ESR) is activated starting from 2° [4] and is only transitory, with the goal of achieving nominal pointing as soon as possible. This conservative design allows for greater power production and therefore significantly reduces the risk of system failure. Additionally, considering the solar array angle as 5° does not lead to an oversizing of the solar array, since the exceeding area with respect to the nominal angle considered as 0° is only 0.38 %. The lifetime degradation can be computed as:

$$L_{life} = (1 - \mathrm{dpy})^{T_{life}} = 0.9061 \tag{36}$$

where T_{life} is the nominal mission duration, 29 months, as initially designed.[32]
Then after computing the end-of-life power given by the solar array finally the total area is estimated:

$$P_{EOL} = L_{life} P_{BOL} = 128\,\mathrm{W\,m^{-2}} \qquad\qquad A_{SA} = \frac{P_{SA}}{P_{EOL}} = 11.8\,\mathrm{m^2} \tag{37}$$

At this stage, a more refined sizing can be performed, knowing the area and the voltage of the single silicon solar cells [34]. The total number of cells that cover the surface is:

$$N_{cells} = \left\lceil \frac{A_{SA}}{A_{cell}} \right\rceil = 4894 \tag{38}$$

From the voltage values of the system (the actual voltage is $V_{sys} = 29.6$ V) and from the actual cell working point ($V_{cell} = 0.404$V) [34], the number of the cells in series is then:

$$N_{series} = \left\lceil \frac{V_{sys}}{V_{cell}} \right\rceil = 74 \tag{39}$$

which is a quite reliable number according with the literature of the mission [34], from which the actual total number of cells is computed:

$$N_{real} = \left\lceil \frac{N_{cells}}{N_{series}} \right\rceil N_{series} = 4958 \tag{40}$$

From this, the real surface area $A_{SA,real} = N_{real} A_{cell} = 11.96\text{m}^2$. The solar array area computed is very similar to that of the final design [34], validating the dimensioning model.

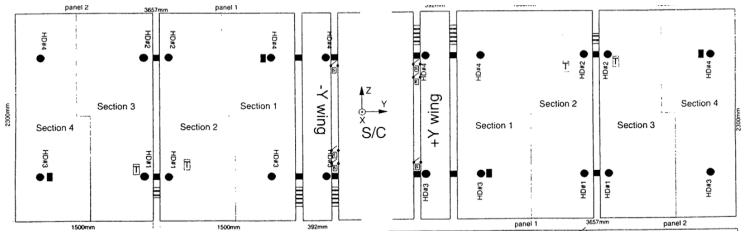

Fig. 13: Solar array dimensions and configuration

7.2.2 Batteries sizing

To size the required charging time of the batteries it was decided to consider a particular case of safe mode whose characteristics are explained below:

- All the payload are switched off to consume the minimum possible power;
- The OBDH subsystem requires a lower amount of power since payloads data are not stored, the percentage of the total budget is computed considering the maximum platform data rate percentage with respect to the maximum payload data rate. [40][44] It can be obtained a 35 % of the power budget reserved for the OBDH subsystem;
- All the eight thrusters are firing during the safe mode to ensure the fastest return in the operational mode.

This is due to the fact that the spacecraft does not have any eclipses during the whole lifetime. Therefore the usage of the batteries is strictly related to an emergency mode in which, since the sun pointing cannot be achieved, the battery module becomes crucial for the survival of the satellite.

PS[40]	**TMTC**[40]	**AOCS**[40]	**TCS**[36]	**P/L**[31]	**Others**[39]	**TOT**	**TOT Margined**
71.4 W	0 W	87 W	303W	0W	61.4 W	525.8W	631 W

Table 38: Subsystems power demand data for emergency mode

The total capacity of the batteries is 950 W h [44]. This allows the system to operate without solar arrays for the time intervals specific for each phase/mode :

Emergency mode:

$$T_{\text{EM}} = \frac{C \cdot \text{DoD} \cdot N_{\text{batt}} \cdot \rho_{\text{discharge}}}{P_{\text{EM}}} = 2.77\,\text{h} \tag{41}$$

ESR mode:

$$T_{\text{ESR}} = \frac{C \cdot \text{DoD} \cdot N_{\text{batt}} \cdot \rho_{\text{discharge}}}{P_{\text{ESR}}} = 1.56\,\text{h} \tag{42}$$

Nominal mode (Maneuver):

$$T_{\text{NOM}} = \frac{C \cdot \text{DoD} \cdot N_{\text{batt}} \cdot \rho_{\text{discharge}}}{P_{\text{NOM}}} = 1.37\,\text{h} \tag{43}$$

Where C represents the total capacity, DoD is the depth of discharge, N_{batt} stands for the number of batteries (2) [35], $\rho_{\text{discharge}}$ denotes the discharge efficiency [35] and P are the respective power demands in each mode.

The DoD is taken as 1 since during all nominal modes the spacecraft faces the sun, generating power from solar arrays, thus not requiring the battery backup. Batteries are just needed (except for rare power peaks) to provide an essential power source in emergency mode. These emergency occasions are limited in number,

thus limiting the number of battery cycles as well. A DoD of 1 can reach up to 1000 cycles [69], which is considerably less than the effective utilization in emergency mode.

The time intervals computed are significantly longer than the possible duration of modes where precise Sun pointing is not feasible, such as during maneuver mode[29], providing a substantial margin for these operations. Furthermore, the battery duration in emergency mode aligns with the actual charge and discharge cycles observed during the SOHO recovery [26]. It is also noteworthy that the SOHO recovery required even less power and did not achieve a full battery charge.

In order to fully characterize the battery, it is necessary to determine the number of cells in series and in parallel, the cells' voltage and their capacity. Starting from the number of cells (32) available [32], it is possible to obtain all these parameters. Given that the maximum voltage delivered by each battery is 47.5 V [32], the only configuration of 32 cells capable of delivering that voltage is having all of them in series. Indeed this would lead to a maximum voltage of:

$$V_{\max} = V_{\text{cell}} \cdot N_{\text{cell, series}} = 48\,\text{V} \tag{44}$$

where the cell voltage V_{cell} is taken as 1.5 V, that is the value to which the Ni-Cd cells can reach up. [78]

This leads to having only one parallel in the design of the battery. Since the system is equipped with two batteries, each has a capacity of half the total $C_{batt} = 475\,\text{W h}$ and therefore this is also the capacity of a single string. It is finally possible to compute the value of required cell capacity:

$$C_{\text{cell}} = \frac{C_{\text{string}}}{\mu \cdot V_{\max}} = 12.5\,\text{A h} \tag{45}$$

where $\mu = 0.8$ is the mean value of package efficiency.
The obtained value is in line with the technology standards. [78]

Another significant information to be determined is the maximum average sun angle at which it would still be possible to recover the satellite, working in the worst-case scenario, which is the Emergency Mode (Em mode). The SAA (θ_{Max}) is computed as follows:

$$P_{\text{EOL, EM}} = \frac{P_{\text{EM}}}{A_{\text{SA, real}}} = 52.77\,\text{W} \qquad P_{\text{BOL, EM}} = \frac{P_{\text{EOL, EM}}}{L_{\text{life}}} = 58.24\,\text{W} \tag{46}$$

$$\theta_{\text{Max}} = \cos^{-1}\left(\frac{P_{\text{bol\_em}}}{P_{\text{in}} \cdot I_{\text{d}}}\right) = 65.75^{\circ} \tag{47}$$

This angle is even larger than the one from which the recovery of SOHO started [75]. This shows the possibility of recovering the satellite even in worse conditions, which could eventually occur if the satellite is not recovered soon enough. Indeed, an eventual uncontrolled motion of the satellite would lead to a sun pointing of the z-axis [68], for which the SAA will be 90°, resulting in zero total power produced by the solar array, leading to mission failure. Therefore a recovery maneuver is mandatory in any case.

A more advanced analysis can be conducted considering the possible shadowing effect of the modules over the solar arrays in a non-nominal condition. This, however, is not taken into account here since the power required is already margined and can be greatly reduced further. This can be achieved by considering shorter cycles in which the battery is only partially charged, allowing critical systems like the Thermal Control System (TCS) to exploit all the remaining power, as it happened during the actual recovery [68].

Batteries are located in the Service module near the Solar array to reduce the amount of wirings used to distribute the power. [39]

7.2.3 System architecture and regulation

The Direct Energy Transfer (DET) method in general offers greater stability, precision, and reliability than Power Peak Tracking (PPT) which is more efficient.
In light of the mission objectives, orbit characteristics and long life a direct energy transfer sun-lit regulated bus would be enough to provide the necessary power to the main components and scientific payloads.

On the other hand, a fully-regulated system is advisable whenever there are modules with a high sensibility to bus voltage and in general to power regulation, such as scientific instruments. Moreover, such a system would be much more robust in case of malfunctions.
For these reasons and considering the high profile of the mission a fully-regulated bus is chosen as it results in an overall sturdier system and comes with a relatively low cost compared to the potential benefits.

7.2.4 Mass and Volume Budgets

Once the surface area of solar panels is obtained through reverse sizing, it is subsequently multiplied by the thickness of each individual cell, including the BSR silicon solar cell and the CMX cover glass, in order to compute the whole panel volume.[34] Then, through the analysis of the specific weight of silicon solar cells, evaluated as 0.3 W/g [42], the mass of a single solar cell and, subsequently, the whole array mass are computed. The obtained result is then added to the mass reserved for the CMX cover glass, evaluated starting from its density value [15]. Based on the fact that interconnection thickness is 10%, the same percentage value is added. Finally, according to [39], a 5% margin is added, while another 5% is added in order to consider the yoke panel contribution.
The mass of the two batteries is then computed considering the minimum value of the specific energy density of Ni-Cd batteries equal to $50\,\mathrm{W\,h\,kg^{-1}}$[55]. The same reasoning is applied for the volume, taking the energy density equal to $200\,\mathrm{W\,h\,L^{-1}}$ [51]. According to [39], 5% margin is added both for the mass and the volume computation as off-the-shelf products without modifications. Finally a further 25 % of the total EPS mass is added considering cables which sustains the power distribution [39]. Since the working voltage of the EPS is quite low (28 V) this percentage was taken as the maximum among the possible choices to have the thickest cables.

Component	**Mass** [kg]	**% Total mass**	**Volume** [m^3]	**% Total Volume**
Solar Array	9.28	0.5	0.0037	0.00861
20 Ah Ni-Cd Batteries	19.95	1.07	0.0050	0.0116
Margin	+25%			
Total	36.54	1.97	0.0109	0.025

Table 39: Mass and Volume Budgets

where the solar array volume and mass values only account for the actual solar cells and the CMX cover glass, thus neglecting the frame structure and the dedicated thermal control system.

This budget estimation does not consider shunt resistors, current limiters and in general all other support electronics, as such an estimate would require a much deeper analysis of the system and precise knowledge of the available components and manufacturers.

7.2.5 Power Budget

The central power regulation is carried out in the Power Control Unit (PCU), whose constant power consumption in standby mode is 5 W. Furthermore, 14 W in standby mode and an additional 8 W for trickle charging are consumed by the Battery Regulator Unit (BRU), that constantly charge and discharge the Ni-Cd Batteries. Finally, the Power Distribution Units (PDU) with four buses each constantly consume 12.5 W. Indeed, when computing the power budget of the EPS, 39.5 W of power consumption have to be taken into account. Then, according to [39], 5% margin is added.

Power Budget W	**% Total Budget**
41.47	2.76

Table 40: Power Budget

7.2.6 Data Budget

To evaluate performance in orbit, we use key power subsystem telemetry parameters. These parameters are collected every 15 s on board, sent to NASA DSN ground stations, and then routed to NASA GSFC for analysis and storage. For long-term evaluation, daily averages from the last day of the month are typically used, unless min-max searches are needed for specific purposes. All analog measurements are converted into 8-bit TM parameters, ensuring $0.53\,\mathrm{bit\,s^{-1}}$ (0.04% of the total housekeeping rate, which includes also attitude sensors), that result to be 0.0057 MB per operational day.

8 Configuration and OBDH subsystem

8.1 Architecture

The design of the SOHO satellite is based on a modular architecture, made of two main components: the Service Module (SVM) and the Payload Module (PLM) connected by a specific adapter (fuchsia in Figure 17). PLM and SVM serve distinct functions and therefore contain elements with different requirements. The adoption of a modular approach down to subsystems level ensures the following benefits:

- Simplified integration and testing by separating the scientific instruments (PLM) from the support systems (SVM);
- Efficient use of space: scientific instruments have specific orientation requirements, while the service systems are arranged to avoid interference.
- Greater flexibility for design changes or upgrades of each module;
- Thermal management: scientific instruments often have specific thermal requirements, which can be more easily managed if they are housed separately from the heat-generating service systems;
- In case of a failure, having a clear separation between the PLM and SVM can help in isolating faults and minimizing the impact on the overall mission.

The SVM itself is divided into two sub-assemblies: the service equipment module and the propulsion module. This facilitates the optimal positioning of the propulsion system tanks, ensuring their alignment with the spacecraft's Center of Mass (CoM), while also maintaining them within specified thermal parameters, being isolated from SVM electronics.

In particular, the Service Module includes the following subsystems [44]:

- Antenna Subsystem (ANTS);
- On-Board Data Handling Subsystem (OBDHS);
- Attitude and Orbit Control Subsystem (AOCS);
- Propulsion Subsystem (PS);
- Electrical Power Subsystem (EPS);
- Payload module Thermal Control Subsystem (PTCS);
- Service module Thermal Control Subsystem (STCS);

Structurally, the SVM is a box-shaped configuration constructed from aluminum honeycomb panels, which are secured to a corrugated aluminum cylinder by four shear webs. The lateral panels of the SVM house the data handling, communication, attitude, orbit control, and power subsystems. [28].

The Payload Module (PLM) features an optical bench dedicated to scientific experiments. It consists of four upper lateral panels and a top panel, all connected to a central cylinder via several shear webs. The lower section of the PLM, comprising three lower lateral panels linked to the central cylindrical tube by shear webs and floors, accommodates the PLM electronics[44] [35]. In this way, a satisfactory thermo-elastic decoupling is obtained, thus avoiding eventual sensors pointing disturbances due to the power dissipation variations imposed by the electronics[28].

8.2 Reverse sizing

8.2.1 Launcher interface and the packed configuration

The launch vehicle adopted for the mission was a two-stage Atlas-IIAS (Atlas/Centaur). The Centaur upper stage is mounted on top of the one-and-one-half-stage Atlas booster, where the SOHO spacecraft is housed.

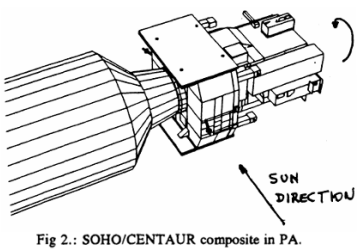

Fig 2.: SOHO/CENTAUR composite in P.A.

Fig. 14: SOHO packed configuration scheme [27]

In particular, it was encapsulated in the payload fairing, which protects the spacecraft through atmospheric ascent up to its release at the end of the parking phase. It consists of a cylindrical section topped by a conical nose cone and a spherical cap. The fairing provides thermal and acoustic enclosures for the payload and launch vehicle electronic compartments during pre-launch and ascent. Portions of the external surface of the fairing are insulated with cork to limit temperatures to acceptable levels. Non-contaminating thermal control coatings are used on internal surfaces to reduce incident heat fluxes to the spacecraft. [7] The spacecraft packed configuration (14) shows significant differences with respect to the nominal configuration in Halo orbit:

- Solar Arrays stowed: ± Y solar panels have no view factor to space as they are folded against the body of the spacecraft;
- CENTAUR and SOHO are attached thanks to the launcher adapter;
- Power dissipation of units is different.

8.2.2 Internal components

Internal elements belong to different subsystems, hence they were mounted in order to achieve field-of-view clearance, pointing stability, and the correct operational temperature.

AOCS: the attitude measurement sensors are installed on the PLM to achieve the highest alignment stability and they are:

- **HR-STR** (yellow in Fig. 16): the star tracker and his redundant counterpart are located in the $+Z$ face of the spacecraft oriented 90° away from the Sun direction and from Earth to avoid, as much as possible, any noise and damage caused from sunlight and from Earth albedo or radiation [3];
- **FPSS**: pointing towards Sun direction ($+X$ axis) [3] to detect sun position with a narrow field of view of $\pm 4.25° \times \pm 4.25°$ [14];
- **FSPAAD** and **CSPAAD**: directed as the aforementioned FPSS towards the Sun direction to exploit their sun acquisition function;
- **RW** (red in Figure 15): pyramid configuration with a redundant wheel. This configuration was chosen to compensate better for the effect around pitch (Y) and yaw (Z) axis, where the biggest component of external disturbances (mainly the solar radiation pressure torque) was expected. The configuration guarantees stabilization also around roll axis (X) but with a less compensation; [27]
- **IMU**: composed by three mechanical gyroscopes oriented as the principal inertia axis of the spacecraft to measure faithfully the respective angular velocities.

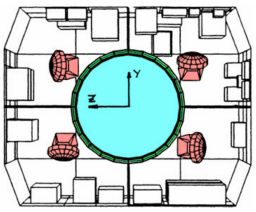

Fig. 15: Internal SVM layout of units [27]

PS: Tank (light blue in Figure 15): the prolate spheroidal tank contains pressurized hydrazine (N_2H_4) and Helium gas (GHe). It is located in the middle of central cylinder of the spacecraft SVM guaranteeing continuous balance around the CoM in case of sloshing due to vibrations. This configuration also allows the CoM to move only along the $+X$ direction. Hydrazine tank has a devoted MLI (green in Figure 15) to minimize the radiative heat interchange with PLM structure, and with the Central Cylinder on the bottom of the S/C. [27]

EPS: batteries, their dedicated regulators, power control unit(PCU) with the dedicated electronics and wirings are contained in the service module.

- **Batteries**: they are located in the Service module near the Solar array to reduce the amount of wirings used to distribute the power. They were mounted as one of the last component to avoid degradation of their performances;[39]
- **PCU** and **PDU**: they are located near the solar panels in order to minimize wiring and in a way that balances out the mass distribution. The high power electronic components is dissipated thanks to the radiators that are located in the near panels.[39]

TCS: the PLM and the SLM have both their own thermal control subsystem, respectively PTCS and STCS.

- **PTCS**: all the instruments (except VIRGO) perform their own thermal control with dedicated heaters and radiators in the related panels: $\pm Z$, $\pm Y$ panels and the $+X$ panel under the sun-shield. Those panels are also directly covered with MLI blankets positioned beneath the radiators; [36]
- **STCS**: the radiators are located on lateral panels and lower platform while what is not covered by radiators is covered with MLI coating. Instead the upper platform is covered by MLI blankets to reduce as much as possible the solar reflection to the PLM while the internal structure uses a black paint coating. [27]

Payload: the overall configuration adopted provides easy mounting and accessibility to the payload instruments, which are housed in the upper module of the spacecraft and arranged on 5 different panels with specific thermal requirements, where their dedicated radiators are placed.

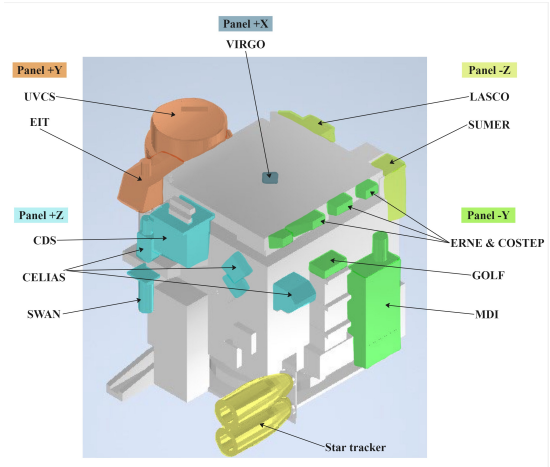

Fig. 16: Payload module components [37]

All the instruments, except for SWAN, point directly to the Sun with their specific accuracy in order to respectively perform helioseismology, coronal, and particles measurements. SWAN is indeed the only remote sensing instrument on SOHO that does not look at the Sun, but it watches the rest of the sky in order to study the interaction between the solar wind and hydrogen coming from interstellar space. [33] The primary focus of the design and layout of the structure is the optimization of the payload instruments' position to facilitate efficient data collection from the Sun. To this purpose, the $+X$ face plays a fundamental role, therefore it is strategically oriented to ensure maximum exposure and unobstructed access to solar data, which is crucial for the primary mission of SOHO. All the external components and other subsystem parts are consequently mounted on the remaining surfaces of the spacecraft. This arrangement ensures that the essential instruments on the $+X$ face are not hindered by any additional equipment, thereby maintaining the integrity and accuracy of the data collection process.

8.2.3 External components

All the external appendages attached to SOHO spacecraft, are placed in specific positions that enable them to complete their tasks successfully:

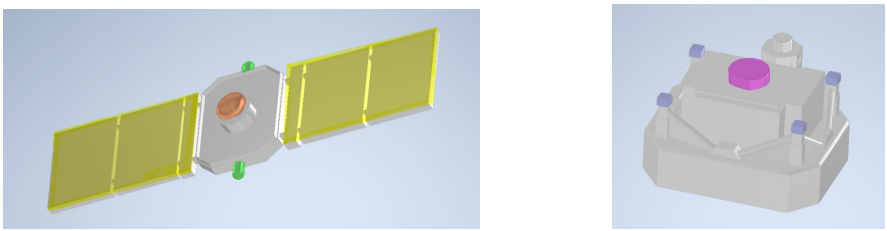

Fig. 17: External components [37]

Thrusters (violet in Figure 17): The sixteen thrusters are arranged into two fully redundant branches of eight thrusters. The primary branch is used for command maneuvers, roll, yaw, and pitch attitude control, while the redundant branch is used mainly in emergency mode. The thruster pairs are placed according to the following configuration:

- 1 and 2 (1 is canted 30° down; 2 at 30° up) are located at Fore(Sunward), giving an impulse in the direction $-X_B$ to control around the Pitch axis;
- 3 and 4 are located at Aft(Earthward), giving an impulse in the direction X_B to control around the Yaw axis;
- 5 and 6 are located at Top($+Z_B$), giving an impulse in the direction $-Z_B$ to control around the Roll axis;
- 7 and 8 are located at Bottom($-Z_B$), giving an impulse in the direction Z_B to control again around the Roll axis;

The inclined thrusters (1 and 2) are partially sun illuminated, 3 and 4 are always in the spacecraft's shadow, and from 5 to 8 are exposed to the sun. All nominal thrust components are in the body XZ plane. This thruster configuration implies that all station-keeping delta-Vs are anti-parallel to the SOHO Sun-line. [57]
Solar Arrays (yellow in Figure 17): they consist of two deployable wings located in the direction $+Y/-Y$, each composed of 2 solar panels and 1 yoke panel. They constantly point towards the Sun ($+X$) with a SAA of 0° to ensure the maximum generated power, this means that they are never in the shadow. To respect one of the mission drivers sun pointing has to be maintained guaranteeing that the SAA remains under two degrees to avoid the start of the safe mode.[4] Their dedicated radiators are placed on the backside of the panel surface.

High Gain Antenna (orange in Figure 17): the HGA is a parabolic antenna, integrated into the spacecraft's central tube. This is placed in the $-X$ face of the spacecraft to ensure continuous communication with the Earth Ground Stations. During normal operations a certain de-pointing of HGA is acceptable, but still needing to be realigned three times per day. The antenna constantly remains in the shadow during the HALO orbit phase.

Low Gain Antennas (green in Figure 17): two additional LGAs ensure omni-coverage. They are quadrifilar short resonant helix antennas. They are installed on the $+Z/-Z$ sides of the satellite, mounted at the bottom section of the service module protruding from the main body to provide full geometrical coverage. Indeed this allows to fill communication gaps when the HGA is not pointing towards Earth, for instance during the emergency mode. [4] The LGAs alternately pass through regions of shadow and sunlit.

8.3 OBDH architecture

SOHO electrical system is organized around two main buses 18: the On-Board Data Handling (OBDH) data link and the 28 V power distribution. The interface between these buses and different subsystems/experiments are performed through standard and identical units: conventional Remote Terminal Units (RTU) for data link and Power Distribution Units (PDU) for power buses.

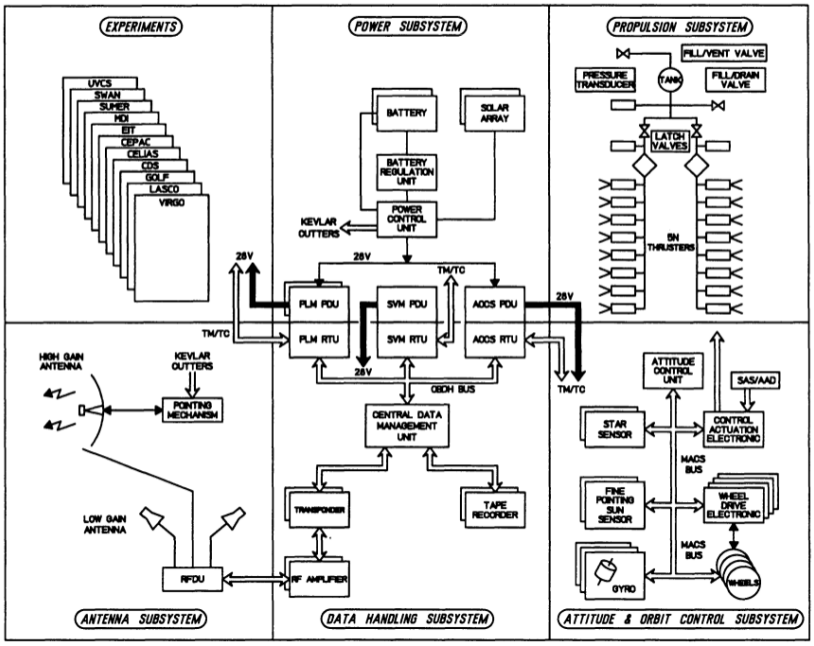

Fig. 18: SOHO electrical block diagram

The heart of the data management and handling system is the Central Data Management Unit (CDMU) which is composed of a redundant intelligent processing unit including a 16 bit MAS281 microprocessor. [18] Among others, this unit is responsible for:

- Data acquisition and formatting from experiments and SVM;
- Data storage during periods of no ground data collection;
- Acquisition, decoding, validation, and distribution of commands from ground to experiments and SVM;
- Maintenance and distribution of time base references for synchronization and time tag purposes;
- Inter-instrument data exchange;
- On-board surveillance and monitoring to ensure the safety of the spacecraft.

The communication between onboard computers and users is realized by the digital OBDH bus which is controlled by the central processor and uses separate lines for interrogation (computer commands or requests) and response (data or acknowledgment to the computer). Therefore, the overall configuration is a federated-bus architecture. This choice enhances reliability and reduces troubleshooting time, which are crucial when managing all the different complex functions required for a mission of this magnitude.

In order to simplify as far as possible the data interfaces, the telemetry and command functions (monitoring, actuating, switching) are combined in three Remote Terminal Units (RTU) which operate under the control of the main computer via the OBDH bus. The RTUs are dedicated respectively to the PLM, the SVM

equipment, and the Attitude Control Unit (ACU). The ACU is based on the same microprocessor as used in the CDMU of the data handling subsystem. The system is fully redundant. Moreover, an independent mode (hardwired) provides a safe mode in failure cases. Two data recorders (one tape recorder of 1 Gbit plus one fully self-redundant solid-state recorder of 2 Gbit capacity) provide the onboard data storage on the non-volatile spacecraft memory. The data are transferred to and from a data recorder on a dedicated link connected to the transfer frame generator.

8.3.1 Reverse Sizing

To estimate the CPU, ROM, and RAM dimensions a sizing by similarity is performed. Firstly all the functions are identified and the acquisition frequencies for all of them are retrieved, specific values were not found in SOHO's literature so the required data have been assumed equal to the typical frequency value associated with each analyzed function or extrapolated from the component's datasheet (RW and sun sensor and both the sun acquisition sensors), in particular, the star tracker acquisition frequency is based on AA-STR and A-STR, whose technology and performances are similar to the SOHO sensor. [24][8][14] Also, the typical throughput for each function is found in the literature [77].

TMTC HGA/LGA/Amplifier/Transponders			
Functions	**Acquisition Frequency** [Hz]	**Typ. Throughput** [KIPS]	**Typical Frequency** [Hz]
Command Processing	10	7.0	10.0
Telemetry Processing	10	3.0	10.0
AODCS Gyroscopes/RW/Thrusters/Sun Sensors/HR-STR			
Functions	**Acquisition Frequency** [Hz]	**Typ. Throughput** [KIPS]	**Typical Frequency** [Hz]
Rate Gyro	10	9.0	10.0
Sun Sensor	10	1.0	1.0
CSPAAD	10	1.0	1.0
FSPAAD	10	1.0	1.0
Star Tracker	10	2.0	0.01
Kinematic Integration	10	15.0	10.0
Error Determination	10	12.0	10.0
Thruster Control	2	1.2	2.0
RW Control	10	5.0	2.0
Ephemeris Propagation	1.0	2.0	1.0
Complex Autonomy	0.5	4.0	0.5
Orbit Propagation	1.0	20.0	1.0
Kalman Filter	0.01	80.0	0.01
TCS Heaters/Radiators			
Functions	**Acquisition Frequency** [Hz]	**Typ. Throughput** [KIPS]	**Typical Frequency** [Hz]
Thermal Control	0.1	3.0	0.1
EPS Solar Panels/Batteries/CPU			
Functions	**Acquisition Frequency** [Hz]	**Typ. Throughput** [KIPS]	**Typical Frequency** [Hz]
Power Management	1	5.0	1
OTHER FUNCTIONS			

Functions	Acquisition Frequency [Hz]	Typ. Throughput [KIPS]	Typical Frequency [Hz]
I/O Device Handlers	5	50	5
Test and Diagnostic	0.1	0.5	0.1
Math Utilities	0.1	0.5	0.1
Executive	10	60	10
Fault Detection	5	15	5
Fault Correction	5	5	5
Complex Autonomy	10	20	10
Monitors	5.0	15.0	5.0
Run Time Kernel	10	60	10

Table 41: Typical Throughput and Frequency and Acquisition Frequency

Also the Kalman filter is assumed to be used in SOHO because of the importance in a rough but useful initial computation of the total state vector or furthermore as an important backup tools to use in safe mode. It is important to stress that the autonomy mode chosen is complex because is more demanding with respect to simple autonomy. Once the functions performed by each subsystem are classified concerning the elements that compose it, it's possible to evaluate the throughput needed by each function, as the total one:

$$\text{KIPS} = \frac{\text{KIPS}_{typ} f_{acq}}{f_{typ}} \qquad \text{KIPS}_{tot} = \sum_{i=1}^{n_{fun}} K_{fun} \cdot \text{KIPS}_{fun} \tag{48}$$

K_{fun} represents the element number associated to each function, and n_{fun} is the whole number of functions. The following summarizes the *KIPS* values obtained for each function and the corresponding total value, to which a 400% margin is added in order to account for the uncertainty and variability in data acquisition. The specific values for each function of code and data are also assumed same as typical quantities found in literature [77].

TMTC				
Element	**Number**	**Code [Words]**	**Data [Words]**	**KIPS**
Command Processing	2	1000	4000	7
Telemetry Processing	2	1000	2500	3
AODCS				
Element	**Number**	**Code [Words]**	**Data [Words]**	**KIPS**
Rate Gyro [40]	3	800	500	9
Sun Sensors [40]	2	500	100	10
CSPAAD [40]	1	500	100	10
FSPAAD [40]	1	500	100	10
HR-STR [40]	2	2000	15000	2000
Kinematic Integration	1	2000	200	15
Error Determination	1	1000	100	12
Thrusters Control[40]	16	600	400	1.2
RW Control [40]	4	1000	300	25
Ephemeris Propagation	1	2000	300	2
Complex Autonomy	1	3500	2500	4

Orbit Propagation	1	13000	4000	20
Kalman Filter	1	8000	1000	80
TCS				
Element	**Number**	**Code[Words]**	**Data[Words]**	**KIPS**
Thermal Control [36]	2	800	1500	3
EPS				
Element	**Number**	**Code [Words]**	**Data [Words]**	**KIPS**
Power Management	1	1200	500	5
OTHER FUNCTIONS				
Element	**Number**	**Code[Words]**	**Data[Words]**	**KIPS**
I/O Device Handlers	1	2000	700	50
Test and Diagnostic	1	700	400	0.5
Math Utilities	1	1200	200	0.5
Executive	1	3500	2000	60
Fault Detection	1	4000	1000	15
Fault Correction	1	2000	10000	5
Complex Autonomy	1	15000	10000	20
Monitors	1	4000	1000	15
Run Time Kernel	1	8000	4000	60
Total		98700	93400	4576.2
+400% Margin		493500	467000	22881

Table 42: Subsystems' Total Code, Data, and KIPS

Because the thermal control system is different between the PLM and SVM, two different thermal controls are considered. It should be noted that typically only a portion of the functions mentioned will be carried out concurrently in each flight mode. However, for the purpose of this analysis, a worst-case scenario is taken into account, meaning that the sizing criteria consider the possibility of all of the previous functions being conducted simultaneously.
Based on the fact that, in orbital maneuver mode EPS, TCT, and TMTC are active and cooperate with both AODCS and PS, we may say that the previous worst-case scenario is a good assumption as it closely mirrors what occurs in reality in the nominal mode.
Finally, considering 16-bit words available from the MAS281 microprocessor, it is possible to evaluate the size of both the ROM and RAM, only after converting total Code and Data words into kB.

$$\text{ROM} = \frac{\text{Code}_{TOT} \cdot 16}{8 \cdot 1000} = 987\,\text{kB} \qquad \text{RAM} = \frac{(\text{Code}_{TOT} + \text{Data}_{TOT}) \cdot 16}{8 \cdot 1000} = 1921\,\text{kB} \tag{49}$$

	ROM [MB]	**RAM [MB]**	**TP [MIPS]**
Real Values	0.144	0.256	-
Computed Values	0.987	1.921	22.81

Table 43: Comparison between real and estimated values

Where real values are computed from [35] using the Equation 49 by considering only one computer containing both AOCS and Data Handling subsystems memory. Comparing the actual values with the values obtained through the sizing process, it is common to notice that the estimated values exceed the pre-established margins. This should not cause dismay, as it was predictable that there would be an overestimation of the results, partly due to the addition of a 400% margin and partly due to the uncertainty of the input data, caused by a lack of reliable references.

References

[1] Leonardo Star Trackers - Flight Experiences and Introduction of SPACESTAR Product on GEO Platforms.
https://indico.esa.int/event/182/contributions/1506/attachments/1456/1682/1710-Boldrini.pdfl.

[2] SOHO (Solar and Heliospheric Observatory).
https://www.eoportal.org/satellite-missions/soho-extended-life-for-esas-science-missions.

[3] SOHO, what happened after 1999? .
https://articles.adsabs.harvard.edu//full/2006ESASP.617E..30V/0000030.006.html.

[4] Spacecraft Emergencies and Pointing Modes.
https://soho.nascom.nasa.gov/soc/esr/.

[5] A Dual Multilayer Insulation Blanket Concept to Radically Reduce Heat Loss From Thermally Controlled Spacecraft and Instruments .
https://ttu-ir.tdl.org/server/api/core/bitstreams/06499af7-6f37-458d-8647-532651f23a61/content .

[6] Antennas of the Deep Space Network.
https://www.nasa.gov/directorates/somd/space-communications-navigation-program/antennas-of-the-dsn/.

[7] Atlas 2as vehicle data.
https://spaceflightnow.com/atlas/ac162/011007atlas2as.html.

[8] AUTONOMOUS STAR TRACKERS.
https://space.leonardo.com/documents/16277711/19573187/Copia$_d i_{AS} TR_A utonomous_S tar_T rackers_L Q_m m077$
1538987562062.

[9] Deep space network services catalog.
https://deepspace.jpl.nasa.gov/files/820-100-H.pdf.

[10] Double Aluminized Kapton® Film .
https://www.dunmore.com/products/double-aluminized-polyimide-film.html.

[11] DuPont™ Kapton®.
https://www.dupont.com/content/dam/dupont/amer/us/en/ei-transformation/public/documents/en/EI-10142-Kapton-Summary-of-Properties.pdf.

[12] Electrodag 501 paint specifications.

[13] ESA space weather, CDF study report .

[14] Fine Pointing Sun Sensor.
https://satsearch.co/products/redwirespace-fine-pointing-sun-sensor.

[15] High efficiency thin-film solar cells for space applications: challenges and opportunities.
https://repository-ubn-ru-nl/bitstream/handle/2066/167041/167041.pdf/.

[16] Indium Tin Oxide (ITO) - Properties and Applications.
https://www.azom.com/article.aspx?ArticleID=2349.

[17] Long Term Missions at the Sun-Earth Libration Point L1: ACE, SOHO, and WIND.
https://core.ac.uk/download/pdf/158348809.pdf.

[18] MAS281 datasheet.
https://datasheetspdf.com/datasheet-pdf/403936/MAS281.html.

[19] More SOHO Recovery Updates .
https://soho.nascom.nasa.gov/operations/Recovery/moreupdates.html .

[20] Mre-1.0 monopropellant thruster.
https://cdn.prd.ngc.agencyq.site/-/media/wp-content/uploads/MRE-10-MonoProp-Thruster.pdf.

[21] Multi-layer insulation. https://en.wikipedia.org/wiki/Multi-layer-insulation.

[22] Optical solar reflector .
https://www.excelitas.com/product/optical-solar-reflectors .

[23] PSG120FD paint specifications. https://www.spacematdb.com/spacemat/datasearch.

[24] Reaction Wheel Unit W18.
https://satsearch.co/products/bradford-reaction-wheel-unit-w18.

[25] S Band Satellite Antennas.
https://www.satnow.com/search/satellite-antennas/ .

[26] Saving SOHO.
https://articles.adsabs.harvard.edu//full/2006ESASP.617E..29V/0000029.003.html.

[27] SOH0 SVM Thermal Control.
https://www.sae.org/publications/technical-papers/content/941427/.

[28] Soho: A modular spacecraft concept to allow flexible payload integration and efficient development.
https://www.sciencedirect.com/science/article/pii/009457659500070G.

[29] SOHO events list .
https://soho.nascom.nasa.gov/soc/soho-events/SOHO-Spacecraft-Events.pdf.

[30] SOHO Mission Interruption Preliminary Status and Background Report - July 15, 1998t.
https://umbra.nascom.nasa.gov/soho/prelim-and-background-rept.html.

[31] SOHO Mission Update.
https://soho2018.sciencesconf.org/data/pages/SOHO-29-SOHO-Status-2018-Fleck.pdf.

[32] SOHO Power System Performance During 6 Years in Orbit.
https://articles.adsabs.harvard.edu//full/2002ESASP.502..141R/0000145.000.html.

[33] SOHO (Solar and Heliospheric Observatory).
https://www.eoportal.org/satellite-missions/soho.

[34] SOHO solar array.
https://adsabs.harvard.edu/full/1998ESASP.416..621R.

[35] The soho spacecraft.
https://www.esa.int/esapub/bulletin/bullet84/vdbus84.htm.

[36] SOHO spacecraft thermal control aspects.
https://articles.adsabs.harvard.edu.

[37] Solar and Heliospheric Observatory. `https://nasa3d.arc.nasa.gov/detail/soho-2`.

[38] Solar radiation in space.
https://www.pveducation.org/pvcdrom/properties-of-sunlight/solar-radiation-in-space.

[39] Space Systems Engineering and Operations slides.

[40] Space Systems Engineering Homework 1-2-3-4-5-6-7.

[41] Thermal emissivity values .
https://www.design1st.com/Design-Resource-Library/engineering-data/ThermalEmissivityValues.pdf.

[42] Ultrathin and lightweight organic solar cells with high flexibility.
https://www.researchgate.net/publication/223985526-Ultrathin-and$_{l}ightweight - organic - solar - cells - with - high - flexibility/$.

[43] P. Michel R. Morgan-Owen A. Winton, J.-L. Gerner. The transponder - a key element in esa spacecraft ttc systems.
https://www.esa.int/esapub/bulletin/bullet86/wint86.htm.

[44] V. Domingo B. Fleck and A. Poland. *The SOHO mission.* Kluwer Academic Publishers, 1995.

[45] C. Berner, V. Domingo. The SOHO Payload and Its Testing.
https://www.esa.int/esapub/bulletin/bullet84/domi84.htm.

[46] ESA. Science operations plan, 1995.

[47] ESA. The soho ground segment and operations, 1995.

[48] ESA. The soho payload and its testing, 1995.

[49] ESA. Soho: Tracking a solar cycle, 2003.

[50] ESA. Soho's recovery – an unprecedented success story, 1999.

[51] A. Muñoz F. Nemry, G. Leduc.
Plug-in Hybrid and Battery-Electric Vehicles: State of the research and development and comparative analysis of energy and cost efficiency.

[52] R.W Farquhar. The flight of isee-3/ice: Origins, mission history, and a legacy.
https://doi.org/10.1007/BF03546336.

[53] M. Di Marco E. Di Litta-G. Guarino S. Mezzasoma G. Orlando G. Baldesi, A. Califano. *Mastersat B: Mission and Analysis Design.* PhD thesis, Università degli Studi di Roma "La Sapienza", 2002.

[54] O. Biblarz G. P. Sutton. *Rocket Propulsion Elements - Ninth Edition.* John Wiley Sons, 2017.

[55] Jürgen Garche and Klaus Brandt. Electrochemical Power Sources: Fundamentals, Systems, and Applications.

[56] H. Fiebrich, J. E. Haines, P. Perol, P. Rumler. Power System Performance of the SOHO Spacecraft During the 1998 Attitude Recovery.

[57] R. D. Headrick and J. N. Rowe. Solar and heliospheric observatory (soho) flight dynamics simulations using matlab.
https://ntrs.nasa.gov/api/citations/19960035757/downloads/19960035757.pdf.

[58] AEROSPACE SPECIFICATION METALS INC. Titanium ti-6al-4v (grade 5), annealed.
https://asm.matweb.com/search/SpecificMaterial.aspbassnum=MTP641.

[59] David F. Everett James Richard Wertz, Jeffery John Puschell.
Space Mission Engineering: The new SMAD. 2011.

[60] Jose L. Garcia. SOHO SVM Thermal Control.

[61] Olwen Morgan and Dennis Meinhardt. Monopropellant selection criteria - hydrazine and other options.
https://www.northropgrumman.com/space/diaphragm-tanks-data-sheets-sorted-by-volume.

[62] NASA. Dsn telecommunications link design handbook.
https://deepspace.jpl.nasa.gov/dsndocs/810-005/203/203C.pdf.

[63] NASA. The soho ground segment and operations.
https://www.esa.int/esapub/bulletin/bullet84/worral84.htm.

[64] NASA. Soho mission : An overview of flight dynamics, 1995.

[65] NASA. Soho transfer trajectory phase, 1997.

[66] NASA. Spacecraft emergencies and pointing modes. an overview.
https://soho.nascom.nasa.gov/soc/esr/.

[67] NASA. Telecommunications description.

[68] Jean-Philippe Olive. *SOHO RECOVERY.* NASA.

[69] SAFT P. Bernard. *Nickel–Cadmium: Sealed.* Elsevier B.V., 2009.

[70] S.V. Haugan T. van Overbeek H. Schweitzer M. Chaloupy P. Brekke, B. Fleck.
SPACE WEATHER EFFECTS ON SOHO AND ITS LEADING ROLE IN THE EARLY-WARNING SYSTEM FOR SPACE WEATHER.

[71] National Aeronautics R. Short, J. Behuncik and USA 20771 Space Administration Goddard Space Flight Center Greenbelt, Maryland. The solar and heliospheric observatory(soho) mission: An overview of flight dynamics support of the early mission phase.
https://ntrs.nasa.gov/api/citations/19960035770/downloads/19960035770.pdf.

[72] Craig E. Roberts. Long term missions at the sun-earth libration point l1: Ace, soho, and wind.
https://core.ac.uk/download/pdf/158348809.pdf.

[73] Craig E. Roberts. The soho mission l1 halo orbit recovery from the attitude control anomalies of 1998.
https://www.researchgate.net/publication/240622471$_{T}he_{S}OHO_{M}ission_{L}1_{H}alo_{O}rbit_{R}ecovery_{F}rom_{t}he_{A}ttitude$

[74] International Telecommunication Union. Radiocommunication requirements for manned and unmanned deep space research.
http://therisingsea.org/notes/FoundationsForCategoryTheory.pdf.

[75] F.C. Vandenbussche. *SOHO's Recovery – An Unprecedented Success Story.* ESA.

[76] W. J. Alldridge. AOCS Technology, 1990.

[77] James R. Wertz Wiley J. Larson. *Space Mission Analysis and Design.* Space Technology Library. Microcosm, 3rd edition, 2005.

[78] Douglas W. Rusta Willard R. Scott.
SEALED-CELL NICKEL-CADIUM BATTERY APPLICATIONS MANUAL. NASA, 1979.